

Effect of the spatial curvature on light bending and time delay in a curved Einstein-Straus–de Sitter spacetime

Mourad Guenouche^{*}

*Laboratoire de Physique Théorique, Université Frères Mentouri-Constantine 1,
BP 325 route de Ain El Bey, 25017 Constantine, Algeria
and Université Abbès Laghrour de Khenchela, BP 1252, El Houria, Route de Constantine,
40004 Khenchela, Algeria*

A method of general applicability has been developed, whereby the null geodesic equations of the Einstein-Straus–de Sitter metric can be integrated simultaneously in terms of the curvature constant k . The purpose is to generalize the computation of light deflection and time delay by a spherical mass distribution. Assuming a flat Universe with most recent measurements of the Hubble constant H_0 and the cosmological constant Λ , five time delays between the four bright images of the lensed quasar SDSS J1004 + 4112 have been forecasted and compared to others in the field, $\Delta t_{DC} = (3250 \pm 64)$ days (8.90 yr), $\Delta t_{DA} = 2049^{+59}_{-58}$ days (5.61 yr), $\Delta t_{AC} = (1269 \pm 77)$ days (3.47 yr), $\Delta t_{BC} = 1176^{+78}_{-77}$ days (3.22 yr), and $\Delta t_{AB} = (93 \pm 70)$ days. This set of time delays constrains the galaxy cluster mass to be $M = (2.447 \pm 0.73) \times 10^{13} M_\odot$. In addition, we have reviewed the question of the possible contribution of a positive Λ to reduce the light bending, and concluded that the changes are seemingly too small to be appreciable on cosmological scales. The same conclusion has been reached regarding the time delay. Having addressed the question of the effect of the spatial curvature in both closed and open Universe, we have found that the strong lensing is slightly affected by the expected small curvature density Ω_{k0} of the current Universe within its error bar $|\Omega_{k0}| \lesssim 0.001$, in such a way that it may safely be neglected. However, it is only if Ω_{k0} gets quite larger that the effect being noticeable. While it is only theoretically possible for Ω_{k0} to be higher, it is worthwhile to stress that this should impact the light bending and time delay, causing them to decrease or increase depending upon whether the spatial curvature is positive or negative. Furthermore, one can infer that the observed light deflection and time delay independently, which are found to be significantly deviated from those of the flat Universe, may serve as a useful means to provide constraints on Ω_{k0} , thus making the approach employed in this work more promising than others.

I. INTRODUCTION

Einstein's general theory of relativity produces two famous testable evidences: the deflection of light near a massive body and the induced time delay. On the occasion of a total solar eclipse in 1919, Eddington had precisely measured the deflection angle due to the Sun, which matched perfectly with what general relativity predicts. The time delay is nothing more than the result of the light ray being longer than it would be without the Sun because of the deflection. This phenomenon is named Shapiro

effect, after the person who discovered it between Earth and Mercury in 1964. In this case, the Sun, or any other star, is said to act as a microlens.

As for the large structures of the Universe, it is a matter of strong and weak lensing effects. Here, it is the strong lensing that we are concerned about. The light coming from background sources is strongly bent by a huge body, modifying the way these sources are seen from Earth and possibly giving rise to multiple images. The lensed quasar SDSS J1004 + 4112 (Sloan Digital Sky Survey) is a case in point. The number and the shape of the images depend on the lens geometry as well as on the source position. Moreover, according to observational measurements, the time delay between some widely separated images may spread over several years.

One of the main aims of this work is to generalize the computation of light deflection and time delay by a spherically symmetric mass distribution in the framework of the Einstein-Straus–de Sitter model (ESdS) [1–4],

^{*}Contact author: guenouche_mourad@umc.edu.dz, guenouche_mourad@univ-khenchela.dz

considering the three possible spatial curvatures of the Friedmann-Lemaître-Robertson-Walker (FLRW) metric: the positively curved space (closed Universe), the negatively curved space (open Universe), and the flat space (Euclidian universe). The choice of this swiss-cheese model is commonly justified by its relevance to the study of the gravitational lensing on cosmological scales. In such a model, the static Schwarzschild–de Sitter (SdS) or Kottler metric inside a vacuole (Schücking sphere) is glued to the homogeneous and isotropic expanding FLRW metric outside. In other words, to be consistent with the observational Hubble law, the model states that the gravitational lensing should only occur inside the vacuole to help explain why the cosmic expansion at larger scales, such as galaxies and clusters, is unobservable at smaller scales, such as planetary and atomic systems. Consequently, the model makes it possible to get rid of many assumptions adopted for simplicity within the SdS model, apart from the spherical symmetry which is of course impossible to overcome [5]. The observer and the source are allowed to be in movement with respect to the galaxy cluster lens as well as be in comovement with respect to a homogeneous isotropic dust including the other galaxy cluster masses, which mostly consists of cold dark matter (CDM). It is worth noting that the spatial curvature outside the vacuole is inherent in the entire FLRW Universe, not to be confused with the curvature of the SdS space-time due to the gravitational field caused by the mass distribution inside the vacuole.

Probing the precise shape of the universe remains an active area of research in cosmology. Observational current data, such as Planck measurements of the cosmic microwave background, indicate that the Universe is dominated by dark energy and CDM, and has a spatial curvature density very close to zero, $\Omega_{k0} = 0.0007 \pm 0.0019$ [6]. That is why most papers often focused on the simplest case of the flat space when dealing with strong lensing, in which the computation of light deflection and time delay is rather simple using features common to the Euclidean space [7–14]. In the nonflat spaces, this ceases to apply, as the photon no longer travels along straight lines outside the vacuole. In Ref. [15], we have already extended the analysis to address the same issue in the case where the expanding FLRW universe is rather positively curved than flat. To accomplish this, we have developed a method relying entirely on Einstein’s postulates of general relativity, which are notoriously accurate in either flat or nonflat space-time. In this paper, we will generalize this method to cover a version of space with a negative curvature constant ($k = -1$), which has not yet been addressed. In this regard, a crucial question naturally arises as to how the light bending and the time delay are affected by the spatial curvature density at the present time and, to be consistent with the observation, whether one could ignore or not this effect in the limit of a weak spatial curvature density.

Not one of cosmologists claims that the time delay does not depend on the cosmological constant Λ , but they do not concur about the real effect on the deflection of light, despite the role that it plays in explaining the dark energy thought to be responsible for the cosmological expansion [16–31]. This question still unsettled is therefore worth further reexamining referring to recent measurements of cosmological parameters.

The paper is organized as follows. Section II is meant to construct the generalized ESdS metric by connecting the Schwarzschild–de Sitter metric with the FLRW one on the vacuole, from which we derive a formula relating the Schwarzschild coordinate time and that of Friedmann, in terms of a constant k uniting both the positive/negative and zero curvature cases. From Sec. III, we get into the details to calculate the deflection of light and the time delay where only the implementation of a method based on integrating differential equations will be relevant to deal with the general case. We devote Sec. IV to validate our theoretical results through numerical applications¹ to the lensed quasar SDSS J1004 + 4112, already evoked above, by addressing each case separately. In the flat case, we provide estimates about the galaxy cluster mass, the deflection angle, and the time delays between the quasar images, and also test them against other recent predictions related to the subject. We also discuss how the light deflection is related to the cosmological constant. In the positively and negatively curved cases, we present a quantitative analysis in order to describe and discuss the evolution of the galaxy cluster mass, the deflection of light and the time delay in terms of the curvature density. In the last section, we end up with conclusions summarizing our main results and open questions offering new perspectives.

II. JUNCTION CONDITIONS FOR GENERALIZED EINSTEIN-STRAUS-DE SITTER METRIC

The first section of this work is about constructing the generalized ESdS metric by linking the SdS and the generalized FLRW metrics, following the same treatment outlined in Refs. [8,10,15]. Let us denote by (T, r, θ, φ) the Schwarzschild coordinates and by $(t, \chi, \theta, \varphi)$ the Friedmann coordinates.

The static Schwarzschild–de Sitter metric takes the form

$$ds_{\text{SdS}}^2 = B(r)dT^2 - B(r)^{-1}dr^2 - r^2d\omega^2, \\ B(r) := 1 - \frac{r_{\text{Schw}}}{r} - \frac{\Lambda}{3}r^2, \quad d\omega^2 = d\theta^2 + \sin^2\theta d\varphi^2, \quad (1)$$

inside a vacuole of radius $r_{\text{Schü}}$, usually named Schücking radius, $(T), r \leq r_{\text{Schü}}$, surrounding a spherical mass

¹All numerical assessments are performed using Wolfram *Mathematica* 11.

distribution M , with $r_{\text{Schw}} := 2GM$ the Schwarzschild radius. The generalized dynamic FLRW metric,

$$ds_{\text{FLRW}}^2 = dt^2 - a(t)^2[d\chi^2 + \mathcal{S}(\chi)^2 d\omega^2], \quad (2)$$

describes the space-time geometry outside the vacuole, $\chi \geq \chi_{\text{Schü}}$, where we define the sine-like function $\mathcal{S}(\chi)$ to facilitate handling all three spatial curvatures simultaneously,

$$\mathcal{S}(\chi) := k^{-1/2} \sin(k^{1/2}\chi) \\ = \begin{cases} \sin \chi & k = +1 \quad (\text{positively curved space}) \\ \chi & k = 0 \quad (\text{flat space}) \\ \sinh \chi & k = -1 \quad (\text{negatively curved space}) \end{cases}, \quad (3)$$

and its cosinelike and tangentlike analogs, $\mathcal{C}(\chi) := \sqrt{1 - k\mathcal{S}(\chi)^2}$ and $\mathcal{T}(\chi) := \mathcal{S}(\chi)/\mathcal{C}(\chi)$. The evolution of the scale factor $a(t)$ over time is governed by the first order Friedmann equation

$$\frac{da}{dt} = aH(a), \quad H(a) := \sqrt{\frac{A}{a^3} - \frac{k}{a^2} + \frac{\Lambda}{3}}, \quad (4)$$

where the function $H(a)$ is the hubble parameter and A is a constant coming from the energy conservation law relative to a nonrelativistic matter-dominated Universe characterized by a pressureless dust with density ρ , $3A := 8\pi G\rho a^3$. Then, $A = (H_0^2 - \Lambda/3)a_0^3 + ka_0$ obtained by writing (4) in the present time, where H_0 is called the hubble constant and a_0 is the scale factor at the present time. It is customary to rearrange the Friedmann equation in the usual standard form in terms of three density parameters: the matter density Ω_ρ , the spatial curvature density Ω_k , and the dark energy (or vacuum) density Ω_Λ as

$$1 = \Omega_\rho + \Omega_k + \Omega_\Lambda, \quad \Omega_\rho = \frac{A}{H(a)^2 a^3}, \\ \Omega_k = \frac{-k}{H(a)^2 a^2}, \quad \Omega_\Lambda = \frac{\Lambda}{3H(a)^2}, \quad (5)$$

with $A := H_0^2 a_0^3 (1 - \Omega_{k0} - \Omega_{\Lambda0})$ rewritten in terms of the present spatial curvature density Ω_{k0} and the present dark energy density $\Omega_{\Lambda0}$.

The two solutions are connected on the vacuole under the matching condition

$$r_{\text{Schü}}(T) := a(t)\mathcal{S}_{\text{Schü}}, \quad (6)$$

with $\mathcal{S}_{\text{Schü}} := \mathcal{S}(\chi_{\text{Schü}})$. Then, using the fact that M , ρ , and $r_{\text{Schü}}$ are related by $3M = 4\pi r_{\text{Schü}}^3 \rho$, the constant Schücking radius can be expressed in terms of A and r_{Schw} as

$$\mathcal{S}_{\text{Schü}} = \left(\frac{r_{\text{Schw}}}{A} \right)^{\frac{1}{3}}. \quad (7)$$

So we have on the vacuole

$$B_{\text{Schü}} := B(r_{\text{Schü}}) = 1 - \left(\frac{A}{a} + \frac{\Lambda}{3} a^2 \right) \mathcal{S}_{\text{Schü}}^2. \quad (8)$$

We will transform the Schwarzschild coordinates (T, r) and the Friedmann coordinates (t, χ) into the new coordinates (b, r) . In this new coordinates, the SdS metric can recast as

$$ds_{\text{SdS}}^2 = B(r)\Psi(b)^2 db^2 - \frac{1}{B(r)} dr^2 - r^2 d\omega^2, \quad (9)$$

by introducing a function $\Psi(b)$ defined as $\Psi(b) := dT/db$. As for the FLRW metric, an intermediate transformation to the coordinates (a, χ) must first be applied using the Friedmann equation (4), before transforming to the new coordinates (b, r) by using

$$a := \Phi(b, r), \quad \mathcal{S}(\chi) := \frac{r}{\Phi(b, r)}. \quad (10)$$

We obtain, after getting rid of mixed terms,

$$ds_{\text{FLRW}}^2 = \left(\frac{\partial \Phi}{\partial b} \right)^2 \frac{1 - [H(\Phi)^2 + k\Phi^{-2}]r^2}{H(\Phi)^2(\Phi^2 - kr^2)} db^2 \\ - \frac{1}{1 - [H(\Phi)^2 + k\Phi^{-2}]r^2} dr^2 - r^2 d\omega^2, \quad (11)$$

with the boundary condition

$$a = b = \Phi(b, b\mathcal{S}_{\text{Schü}}), \quad (12)$$

that at the Schücking radius, old and new time coordinates coincide. We get, by differentiating with respect to b ,

$$\left. \frac{\partial \Phi}{\partial b} \right|_{\text{Schü}} = 1 - \left. \frac{\partial \Phi}{\partial r} \right|_{\text{Schü}} \mathcal{S}_{\text{Schü}} = \frac{\mathcal{C}_{\text{Schü}}^2}{B_{\text{Schü}}(b)}, \quad (13)$$

where $\mathcal{C}_{\text{Schü}} := \mathcal{C}(\chi_{\text{Schü}})$, and $\partial \Phi / \partial r$ is given by

$$\frac{\partial \Phi}{\partial r} = - \frac{\Phi H(\Phi)^2 r}{1 - [H(\Phi)^2 + k\Phi^{-2}]r^2}. \quad (14)$$

The continuity condition is insured by equating the SdS metric components with those of FLRW at the Schücking radius. This requires

$$\Psi(b) = \frac{\mathcal{C}_{\text{Schü}}}{bH(b)B_{\text{Schü}}(b)}. \quad (15)$$

Now, the use of the chain rule allows us to calculate the Jacobian of the transformation from the Schwarzschild coordinates to the Friedmann coordinates at the Schücking radius, i.e.,

$$\left. \frac{\partial t}{\partial T} \right|_{\text{Schü}} = \mathcal{C}_{\text{Schü}}, \quad \left. \frac{\partial t}{\partial r} \right|_{\text{Schü}} = -\frac{aH(a)\mathcal{S}_{\text{Schü}}}{B_{\text{Schü}}},$$

$$\left. \frac{\partial \chi}{\partial T} \right|_{\text{Schü}} = -H(a)\mathcal{S}_{\text{Schü}}, \quad \left. \frac{\partial \chi}{\partial r} \right|_{\text{Schü}} = \frac{\mathcal{C}_{\text{Schü}}}{aB_{\text{Schü}}}. \quad (16)$$

Finally, considering the parametrized curve, $T = p$, $r = b\mathcal{S}_{\text{Schü}}$ ($\theta = \pi/2$, $\varphi = 0$) and calculating its 4-velocity, one can easily relate the Schwarzschild coordinate time T to that of Friedmann t on the vacuole. The resulting relationship is

$$\left. \frac{dt}{dT} \right|_{\text{Schü}} = \frac{dt}{dp} \frac{dp}{dT} = \frac{B_{\text{Schü}}}{\mathcal{C}_{\text{Schü}}}, \quad (17)$$

which ensure smooth passage of photons through the boundary between the SdS and FLRW geometries and vice versa.

III. DEFLECTION OF LIGHT AND TIME DELAY

We suggest to study a typical scenario, as shown in Fig. 1, in which two photons are emitted by a source S at times t_S and t'_S , enter the vacuole on one side at $t_{\text{SchüS}}$ and $t'_{\text{SchüS}}$, exit it on the other side at $t_{\text{SchüE}}$ and $t'_{\text{SchüE}}$, and eventually reach the Earth E at the same time $t_E = t'_E = 0$, where the final FLRW-type conditions are well known. It seems therefore more practical to carry out the integration of null geodesic equations backward in time, from the Earth to the vacuole, inside the vacuole, and from the vacuole to the source. Meanwhile, the use of the Jacobian transformation as well as its inverse are indispensable to convert the initial FLRW-type conditions to the final SdS-type conditions on the vacuole in front of the Earth, and the initial SdS-type conditions to the final FLRW-type conditions on the vacuole in front of the source. An added advantage of such a situation is that the time delay between both photons—difference between their total travel times from the emission times on the source to the receipt times being synchronized on Earth—will be simply expressed as $\Delta t := \Delta t_S := t_S - t'_S$. We denote by α and α' the angles that the two photons make upon receipt on Earth with the

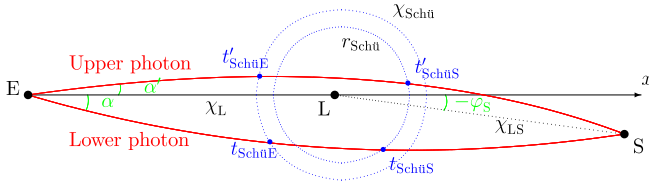


FIG. 1. Two photons emitted by a source S , bent inside the vacuole and finally received at Earth E . The trajectories outside the vacuole converge in the case of a spherical geometry of positive curvature, while they diverge in the case of a hyperbolic geometry of negative curvature. In a flat geometry, they are straight lines. We have limited ourselves to the spherical case to avoid overloading the figure.

Earth-lens axis, and by r_P and r'_P , the minimum approach distances (perilens) at which they get deflected by the lens L .

It is important to note that even though the Friedmann equation (4) can be analytically solved in the case of nonzero curvature, with the aid of elliptic integrals of the second and third kinds, to provide the cosmic time $t(a)$ and the inverse function for the scale factor $a(t)$, which is still unknown in terms of the curvature constant k , unless in the case of a flat space $k = 0$ [10]. Instead, one can opt to solve the problem by means of the numerical integration method.

The numerical integration of the radial null geodesic equation

$$d\chi = -\frac{dt}{a(t)} \quad (18)$$

is also necessary to calculate the Earth-lens and the Earth-source geodesic distances, χ_L and χ_S , where only the minus sign must be retained since the origin is defined on Earth, $\chi(t=0) = 0$, leading to an increasing geodesic distance $\chi(t)$ over time. But, this equation involves $a(t)$, which is only analytically known in the case $k = 0$. In response to such a problem, one could introduce the Hubble parameter $H(a)$ and the cosmological redshift z via the Friedmann equation (4) and the well-known formula $1 + z = a_0/a$ in order to integrate with respect to the scale factor,

$$\chi(z) = \int_{\frac{a_0}{1+z}}^{a_0} \frac{da}{a^2 H(a)}, \quad (19)$$

or with respect to z ,

$$\chi(z) = \int_z^0 \frac{dz}{a_0 H(z)},$$

$$H(z) = H_0 \sqrt{\Omega_{\rho 0}(1+z)^3 + \Omega_{k0}(1+z)^2 + \Omega_{\Lambda 0}}. \quad (20)$$

Hence, χ_L and χ_S will be calculated for any given value of z_L and z_S ; $\chi_L := \chi(z_L)$ and $\chi_S := \chi(z_S)$. Concerning the geodesic distance that joins the lens to the source χ_{LS} , it can be approximated as being aligned with χ_L ,

$$\chi_{LS} \simeq \chi_S - \chi_L, \quad (21)$$

due to the small $-\varphi_S$ of the order of a few arc seconds ($\sim 10^{-5}$).

A. Integration of null geodesic equations between the Earth and the vacuole

In this region, where the generalized FLRW metric (2) prevails, two geodesic equations are sufficient to describe the photon trajectory in the equatorial plane $\theta = \pi/2$,

$$i\ddot{t} + a\dot{a}[\dot{\chi}^2 + \mathcal{S}(\chi)^2\dot{\varphi}^2] = 0, \quad (22)$$

$$\frac{1}{2}\ddot{\varphi} + \frac{\dot{a}}{a} + \frac{\dot{\chi}}{T(\chi)} = 0, \quad (23)$$

where the dot denotes differentiation with respect to p , an affine parameter other than s since the photon moves along null geodesics $ds = 0$.

The final FLRW-type conditions of the upper photon upon arrival on Earth ($t = 0, \chi = \chi_L, \varphi = \pi$) are given by its 4-velocity

$$\dot{t} = 1, \quad \dot{\chi} = \frac{\cos \beta'}{a_0}, \quad \dot{\varphi} = \frac{\sin \beta'}{a_0 \mathcal{S}_L}, \quad (24)$$

where we have used the fact that the physical angle α' coincides with the coordinate angle $\arctan(\mathcal{T}_L |d\varphi/d\chi|_{\chi_L})$, and defined the constant β' by $\tan \beta' := \mathcal{C}_L \tan \alpha'$, with $\mathcal{S}_L := \mathcal{S}(\chi_L)$, $\mathcal{C}_L := \mathcal{C}(\chi_L)$, and $\mathcal{T}_L := \mathcal{T}(\chi_L)$. These final FLRW-type conditions permit a straightforward integration of (22) and (23) to get

$$t = \frac{a_0}{a(t)}, \quad \varphi = \frac{a_0 \mathcal{S}'_{PE}}{a^2 \mathcal{S}(\chi)^2}, \quad \varphi = \pi - \arcsin \frac{\mathcal{T}'_{PE}}{\mathcal{T}(\chi)} + \beta', \quad (25)$$

where the perilens χ'_{PE} is defined such that \mathcal{S}'_{PE} , \mathcal{C}'_{PE} , and \mathcal{T}'_{PE} are related to each other by $\mathcal{S}'_{PE} := \mathcal{S}(\chi'_{PE}) := \mathcal{S}_L \sin \beta'$, $\mathcal{C}'_{PE} := \mathcal{C}(\chi'_{PE}) := \sqrt{\cos^2 \beta' + \mathcal{C}_L^2 \sin^2 \beta'}$, and $\mathcal{T}'_{PE} := \mathcal{T}(\chi'_{PE}) = \mathcal{S}'_{PE}/\mathcal{C}'_{PE}$.

Now, we are going to follow the approach originally proposed in Ref. [15], in order to determine the scale factor $a'_{SchüE}$ and its corresponding time $t'_{SchüE}$, at which the upper photon emerges from the vacuole. What we know up to now are the constant Schücking radius $\chi_{Schü}$ and its corresponding polar angle $\varphi'_{SchüE} := \varphi(\chi_{Schü})$ via the relationship between χ and φ (25). So the idea is to relate one of them with time, $\chi(t)$ or $\varphi(t)$. Removing the affine parameter between \dot{t} and $\dot{\varphi}$ in (25) and injecting the result into the generalized FLRW metric (2) for a photon, we get immediately

$$\frac{dt}{a(t)} = \frac{d\chi}{g(\chi)}, \quad g(\chi) := \sqrt{1 - \frac{\mathcal{S}_{PE}^2}{\mathcal{S}(\chi)^2}}, \quad (26)$$

where we have taken into account that $\chi(t)$ is a decreasing function of time in this region. The left-hand side of this equation comprises $a(t)$ which we fail to know in the general case, as said before. So we should instead integrate with respect to the scale factor by inserting the Hubble parameter $H(a)$ through the Friedmann equation (4). The integration of the right-hand side can be analytically carried out to provide the function $-k^{-1/2} \arcsin[\mathcal{C}(\chi)/\mathcal{C}'_{PE}]$ and evaluated between the vacuole and the Earth to provide the geodesic distance traveled by the photon. The result is

$$\int_{a'_{SchüE}}^{a_0} \frac{da}{a^2 H(a)} = k^{-1/2} \left(\arcsin \frac{\mathcal{C}_{Schü}}{\mathcal{C}'_{PE}} - \arcsin \frac{\mathcal{C}_L}{\mathcal{C}'_{PE}} \right), \quad (27)$$

which enables us to obtain $a'_{SchüE}$ by numerical integration. The corresponding value of $t'_{SchüE}$ is then calculated by numerical integration of the Friedmann equation, i.e.,

$$t'_{SchüE} = \int_{a_0}^{a'_{SchüE}} \frac{da}{aH(a)}, \quad (28)$$

if one is interested in that. Let us note that the right-hand side of (27) reduces to

$$\text{rhs}(k=0) = \sqrt{\chi_L^2 - \chi_{PE}^2} - \sqrt{\chi_{Schü}^2 - \chi_{PE}^2}, \quad (29)$$

equivalent to the result of Refs. [8,10] in the flat case $k=0$, and to the result of Ref. [15] in the closed case $k=+1$. In the hyperbolic case $k=-1$, it reduces to

$$\text{rhs}(k=-1) = \text{arccosh} \frac{\cosh \chi_L}{\cosh \chi'_{PE}} - \text{arccosh} \frac{\cosh \chi_{Schü}}{\cosh \chi'_{PE}}. \quad (30)$$

The time $t_{SchüE}$, at which the lower photon emerges from the vacuole, can be calculated in the same manner as before, using similar formulas. We just have to replace α' by $-\alpha$ as well as the polar angle π by $-\pi$ on Earth.

However, we can proceed, in a way analogous to the flat and closed cases [10,15], to develop an analytical approximate expression of the time delay between the two photons at the exit from the vacuole, i.e., $\Delta t_{SchüE} := t_{SchüE} - t'_{SchüE}$. Subtracting the right and the left-hand side of (27) from the ones which correspond to the lower photon, one gets

$$\int_{t'_{SchüE}}^{t_{SchüE}} \frac{dt}{a(t)} = k^{-1/2} \left(\arcsin \frac{\mathcal{C}_{Schü}}{\mathcal{C}'_{PE}} - \arcsin \frac{\mathcal{C}_L}{\mathcal{C}'_{PE}} - \frac{\mathcal{C}_{Schü}}{\mathcal{C}_{PE}} + \arcsin \frac{\mathcal{C}_L}{\mathcal{C}_{PE}} \right). \quad (31)$$

The left-hand side of this equation can be approximated using the fact that the scale factor varies significantly only on cosmological timescales, i.e.,

$$\text{lhs} \simeq \frac{\Delta t_{SchüE}}{a'_{SchüE}}, \quad (32)$$

while an expansion of the right-hand side to the second-to-leading order in \mathcal{S}'_{PE} and \mathcal{S}_{PE} ($\sim 10^{-6}$) or in α' and α ($\sim 10^{-5}$) can be carried out to give

$$\text{rhs} \simeq \frac{1}{2} (\mathcal{T}_{Schü}^{-1} - \mathcal{T}_L^{-1}) \mathcal{S}_L^2 \mathcal{C}_L^2 (\alpha'^2 - \alpha^2), \quad (33)$$

where $T_{\text{Schü}} := \mathcal{T}(\chi_{\text{Schü}})$. Equating the two sides, we get

$$\Delta t_{\text{SchüE}} \simeq \frac{1}{2} a'_{\text{SchüE}} (T_{\text{Schü}}^{-1} - T_{\text{L}}^{-1}) \mathcal{S}_{\text{L}}^2 \mathcal{C}_{\text{L}}^2 (\alpha'^2 - \alpha^2). \quad (34)$$

Particularly, this is negative for $\alpha' < \alpha$, meaning that the lower photon precedes the upper one at the exit from the vacuole before they are received all together on Earth.

One can easily recover the results of the flat and the closed ESdS models in Refs. [10,15], taking $k = 0$ and $k = +1$, as well as the result of the open ESdS model, taking $k = -1$,

$$\Delta t_{\text{SchüE}} \simeq \frac{1}{2} a'_{\text{SchüE}} (\coth \chi_{\text{Schü}} - \coth \chi_{\text{L}}) \sinh^2 \chi_{\text{L}} \cosh^2 \chi_{\text{L}} (\alpha'^2 - \alpha^2). \quad (35)$$

B. Integration of null geodesic equations inside the vacuole

At this step when the two photons permeate through the SdS space-time, the formulas that we are going to employ are extremely similar to those used in the flat and closed ESdS cases [10,15]. The only difference arises from the use of the relationship between the Schwarzschild time T and the Friedmann time t (17), which brings out the curvature constant k . We will therefore emphasize only what we need to calculate the time delay between the two photons at the entry into the vacuole represented by $\Delta t_{\text{SchüS}} := t_{\text{SchüS}} - t'_{\text{SchüS}}$.

Let us first determine the time it takes the upper photon for crossing the vacuole. Thanks to the relationship (17), this travel time can be expressed in terms of $t'_{\text{SchüE}}$ and $t'_{\text{SchüS}}$ as

$$T'_{\text{SchüE}} - T'_{\text{SchüS}} = \mathcal{C}_{\text{Schü}} \int_{t'_{\text{SchüS}}}^{t'_{\text{SchüE}}} \frac{dt}{B_{\text{Schü}}(t)}. \quad (36)$$

The same quantity can be expressed otherwise by making use of the two well-known partially integrated geodesic equations of the SdS space-time (1),

$$\dot{T} = \frac{1}{B(r)}, \quad \dot{r} = \pm \sqrt{1 - J'^2 \frac{B(r)}{r^2}}, \quad (37)$$

with J' a constant of motion defined by $J' = r'_p / \sqrt{B(r'_p)}$ and interpreted as an angular momentum per unit mass, r'_p the perilens given approximately by $r'_p \simeq r'_{\text{SchüE}} \sin \gamma'_{\text{SdS}} - r_{\text{Schw}}/2$ [8], where γ'_{SdS} denotes the smaller coordinate angle between the unoriented direction of the upper photon and the direction toward the lens, i.e., $\gamma'_{\text{SdS}} := \arctan |r'_{\text{SchüE}} \dot{\phi}'_{\text{SchüE}} / \dot{r}'_{\text{SchüE}}|$, with $r'_{\text{SchüE}} := a'_{\text{SchüE}} \mathcal{S}_{\text{Schü}}$ (6), $\dot{\phi}'_{\text{SchüE}} := \dot{\phi}(r'_{\text{SchüE}})$ (25), and $\dot{r}'_{\text{SchüE}}$ calculated in terms of $\dot{t}_{\text{SchüE}}$ and $\dot{\chi}_{\text{SchüE}}$ using the inverse Jacobian of (16). Eliminating the affine parameter between \dot{T} and \dot{r} in (37), we find

$$dT = \pm \frac{dr}{v'(r)}, \quad v'(r) := B(r) \sqrt{1 - J'^2 \frac{B(r)}{r^2}}, \quad (38)$$

which gives

$$T'_{\text{SchüE}} - T'_{\text{SchüS}} = \left(\int_{r'_p}^{r'_{\text{SchüE}}} + \int_{r'_p}^{r'_{\text{SchüS}}} \right) \frac{dr}{v'(r)}, \quad (39)$$

using the fact that r decreases with time from $r'_{\text{SchüS}}$ to r'_p while it increases from r'_p to $r'_{\text{SchüE}}$. It follows from (36) and (39) that

$$\left(\int_{r'_p}^{r'_{\text{SchüE}}} \mathcal{S}_{\text{Schü}} + \int_{r'_p}^{r'_{\text{SchüS}}} \mathcal{S}_{\text{Schü}} \right) \frac{dr}{v'(r)} = \mathcal{C}_{\text{Schü}} \int_{a'_{\text{SchüS}}}^{a'_{\text{SchüE}}} \frac{da}{a H(a) B_{\text{Schü}}(a)}, \quad (40)$$

where we have, as before, inserted the hubble parameter through the Friedmann equation in order to make possible the integration with respect to the scale factor, with $r'_{\text{SchüS}} := a'_{\text{SchüS}} \mathcal{S}_{\text{Schü}}$. This equation can be numerically solved to yield the value of $a'_{\text{SchüE}}$. If one is interested in $t'_{\text{SchüS}}$, then one can numerically integrate the Friedmann equation, i.e.,

$$t'_{\text{SchüS}} = \int_{a_0}^{a'_{\text{SchüS}}} \frac{da}{aH(a)}. \quad (41)$$

Similar formulas are applied leading to the calculation of the scale factor $a_{\text{SchüS}}$ when the lower photon immerses into the vacuole.

Let us now develop an analytical approximate expression for $\Delta t_{\text{SchüS}}$ following the same method described in Refs. [10,15]. We make use of the relationship (17) to write

$$\begin{aligned} \Delta T_{\text{SchüE}} - \Delta T_{\text{SchüS}} &= C_{\text{Schü}} \left(\int_{t'_{\text{SchüE}}}^{t_{\text{SchüE}}} - \int_{t'_{\text{SchüS}}}^{t_{\text{SchüS}}} \right) \frac{dt}{B_{\text{Schü}}(t)} \\ &\simeq C_{\text{Schü}} \left(\frac{\Delta t_{\text{SchüE}}}{B'_{\text{SchüE}}} - \frac{\Delta t_{\text{SchüS}}}{B'_{\text{SchüS}}} \right), \end{aligned} \quad (42)$$

taking into account that $B_{\text{Schü}}$ is only significant on cosmological timescales, with $\Delta T_{\text{SchüE}} := T_{\text{SchüE}} - T'_{\text{SchüE}}$, $\Delta T_{\text{SchüS}} := T_{\text{SchüS}} - T'_{\text{SchüS}}$, $B'_{\text{SchüE}} := B_{\text{Schü}}(t'_{\text{SchüE}})$, and $B'_{\text{SchüS}} := B_{\text{Schü}}(t'_{\text{SchüS}})$. In fact, this express the difference in the travel times between both photons inside the vacuole. This latter could be written in a different way (differently) by making use of (38) for the upper photon and its analogous formula for the lower one, i.e.,

$$\Delta T_{\text{SchüE}} - \Delta T_{\text{SchüS}} = \left(\int_{r'_{\text{SchüE}}}^{r_{\text{SchüE}}} + \int_{r'_{\text{SchüS}}}^{r_{\text{SchüS}}} \right) \frac{dr}{v'(r)} - \Delta T_{\text{SdS}}, \quad (43)$$

where we have split up the integrals in such a way as to produce the following expression:

$$\Delta T_{\text{SdS}} := \left(\int_{r'_p}^{r'_{\text{SchüE}}} + \int_{r'_p}^{r'_{\text{SchüS}}} \right) \frac{dr}{v'(r)} - \left(\int_{r_p}^{r_{\text{SchüE}}} + \int_{r_p}^{r_{\text{SchüS}}} \right) \frac{dr}{v(r)}, \quad (44)$$

which can be compared to an expression already involved in the calculation of the time delay in the framework of the Schwarzschild–de Sitter solution [32], i.e.,

$$\begin{aligned} \Delta T_{\text{SdS}} &\simeq \frac{1}{2} (r_p^2 - r_p'^2) \left(\frac{1}{r'_{\text{SchüE}}} + \frac{1}{r'_{\text{SchüS}}} \right) + 2r_{\text{Schw}} \ln \frac{r_p}{r'_p} - \frac{3}{8} \left(1 - \frac{r_p'^2}{r_p^2} \right) \\ &\quad \times \frac{r_{\text{Schw}}^2}{r_p'^2} \sqrt{\frac{3}{\Lambda}} \left[\text{arctanh} \left(\sqrt{\frac{\Lambda}{3}} r'_{\text{SchüE}} \right) + \text{arctanh} \left(\sqrt{\frac{\Lambda}{3}} r'_{\text{SchüS}} \right) \right]. \end{aligned} \quad (45)$$

Furthermore, since the lengths and timescales that we are dealing with are smaller than cosmological ones, the first term on the right-hand side of (43) can be approximated by

$$\begin{aligned} \left(\int_{r'_{\text{SchüE}}}^{r_{\text{SchüE}}} + \int_{r'_{\text{SchüS}}}^{r_{\text{SchüS}}} \right) \frac{dr}{v'(r)} &\simeq \frac{\Delta r_{\text{SchüE}}}{v'_{\text{SchüE}}} + \frac{\Delta r_{\text{SchüS}}}{v'_{\text{SchüS}}} \\ &\simeq \left(\frac{\Delta a_{\text{SchüE}}}{v'_{\text{SchüE}}} + \frac{\Delta a_{\text{SchüS}}}{v'_{\text{SchüS}}} \right) \mathcal{S}_{\text{Schü}} \\ &\simeq \frac{H'_{\text{SchüE}} r'_{\text{SchüE}} \Delta t_{\text{SchüE}}}{v'_{\text{SchüE}}} + \frac{H'_{\text{SchüS}} r'_{\text{SchüS}} \Delta t_{\text{SchüS}}}{v'_{\text{SchüS}}}, \end{aligned} \quad (46)$$

where we have used the matching condition (6) and the Friedmann equation with $\Delta r_{\text{SchüE}} := r_{\text{SchüE}} - r'_{\text{SchüE}}$, $\Delta r_{\text{SchüS}} := r_{\text{SchüS}} - r'_{\text{SchüS}}$, $\Delta a_{\text{SchüE}} := a_{\text{SchüE}} - a'_{\text{SchüE}}$, $\Delta a_{\text{SchüS}} := a_{\text{SchüS}} - a'_{\text{SchüS}}$, $v'_{\text{SchüE}} := v'(r'_{\text{SchüE}})$, $v'_{\text{SchüS}} := v'(r'_{\text{SchüS}})$, $H'_{\text{SchüE}} := H(a'_{\text{SchüE}})$, and $H'_{\text{SchüS}} := H(a'_{\text{SchüS}})$. Using this together with (45), (43), and (42), we therefore get

$$\Delta t_{\text{SchüS}} \simeq \frac{\Delta T_{\text{SdS}} + (B'^{-1}_{\text{SchüE}} C_{\text{Schü}} - H'_{\text{SchüE}} v'^{-1}_{\text{SchüE}} r'_{\text{SchüE}}) \Delta t_{\text{SchüE}}}{B'^{-1}_{\text{SchüS}} C_{\text{Schü}} + v'^{-1}_{\text{SchüS}} H'_{\text{SchüS}} r'_{\text{SchüS}}}. \quad (47)$$

Of course, this result generates what has been obtained in the flat and closed ESdS models [10,15], as well as that of the hyperbolic ESdS model,

$$\Delta t_{\text{Sch\"us}} \simeq \frac{\Delta T_{\text{SdS}} + (B_{\text{Sch\"uE}}'^{-1} \cosh \chi_{\text{Sch\"u}} - H_{\text{Sch\"uE}}' v_{\text{Sch\"uE}}'^{-1} a_{\text{Sch\"uE}}' \sinh \chi_{\text{Sch\"u}}) \Delta t_{\text{Sch\"uE}}}{B_{\text{Sch\"uS}}'^{-1} \cosh \chi_{\text{Sch\"u}} + v_{\text{Sch\"uS}}'^{-1} H_{\text{Sch\"uS}}' a_{\text{Sch\"uS}}' \sinh \chi_{\text{Sch\"u}}}. \quad (48)$$

Remarkably, $\Delta t_{\text{Sch\"us}}$ is positive if $\alpha' < \alpha$, contrary to $\Delta t_{\text{Sch\"uE}}$. This will be explained later, once the total time delay Δt have been calculated.

We close this section by calculating the polar angles $\varphi'_{\text{Sch\"uS}}$ and $\varphi_{\text{Sch\"uS}}$ needed for the next section, at which the upper and lower photons penetrate into the vacuole. We shall exploit the third well-known equation, which for the upper photon reads

$$d\varphi = \pm \frac{dr}{u'(r)}, \quad u'(r) := r \sqrt{\frac{r^2}{r_{\text{P}}^2} - 1} \sqrt{1 - \frac{r_{\text{Schw}}}{r_{\text{P}}} \left(\frac{r_{\text{P}}'}{r} + \frac{1}{1 + r_{\text{P}}'/r} \right)}. \quad (49)$$

This results from eliminating the affine parameter between \dot{r} in (37) and $\dot{\varphi}$ of the third well known partially integrated geodesic equation,

$$\dot{\varphi} = J'/r^2, \quad (50)$$

where the cosmological constant Λ is incidentally erased. The integration of the above equation leads to

$$\varphi'_{\text{Sch\"uE}} - \varphi'_{\text{Sch\"uS}} = \left(\int_{r_{\text{P}}}^{r'_{\text{Sch\"uE}}} + \int_{r_{\text{P}}}^{r'_{\text{Sch\"uS}}} \right) \frac{dr}{u'(r)}, \quad (51)$$

taking into account that φ increases when the upper photon approaches the lens as well as when it moves away. This gives, to the first leading order in the ratio $r_{\text{Schw}}/r_{\text{P}}$,

$$\begin{aligned} \varphi'_{\text{Sch\"uS}} &\simeq \varphi'_{\text{Sch\"uE}} - \pi + \arcsin \frac{r_{\text{P}}'}{r'_{\text{Sch\"uE}}} + \arcsin \frac{r_{\text{P}}'}{r'_{\text{Sch\"uS}}} \\ &\quad - \frac{r_{\text{Schw}}}{2r_{\text{P}}} \left[\left(1 + \frac{1}{1 + r_{\text{P}}'/r'_{\text{Sch\"uE}}} \right) \sqrt{1 - \frac{r_{\text{P}}'^2}{r_{\text{Sch\"uE}}'^2}} \right. \\ &\quad \left. + \left(1 + \frac{1}{1 + r_{\text{P}}'/r'_{\text{Sch\"uS}}} \right) \sqrt{1 - \frac{r_{\text{P}}'^2}{r_{\text{Sch\"uS}}'^2}} \right]. \end{aligned} \quad (52)$$

In the same manner, we obtain a similar expression for the lower photon, where $\varphi_{\text{Sch\"uS}}$ and $\varphi_{\text{Sch\"uE}}$ differ from those of the upper one by a minus sign.

C. Integration of null geodesic equations between the vacuole and the source

In this part of space-time, the motion of photons are ruled by the same geodesic equations of the FLRW metric, (22) and (23). To integrate them, we shall adopt the same technique previously developed in Sec. III A, taking into account the final FLRW-type conditions of the upper photon at the entry into the vacuole ($t = t'_{\text{Sch\"uS}}$, $\chi = \chi_{\text{Sch\"u}}$, $\varphi = \varphi'_{\text{Sch\"uS}}$), i.e.,

$$\dot{t} = \dot{t}'_{\text{Sch\"uS}}, \quad \dot{\chi} = \dot{\chi}'_{\text{Sch\"uS}}, \quad \dot{\varphi} = \dot{\varphi}'_{\text{Sch\"uS}}. \quad (53)$$

These final FLRW-type conditions are calculated by converting the initial SdS-type conditions ($\dot{T}'_{\text{Sch\"uS}}$, $\dot{r}'_{\text{Sch\"uS}}$) (37) using the Jacobian (16). We obtain

$$\begin{aligned} \dot{t} &= \frac{E'}{a(t)}, \quad \dot{\varphi} = \frac{J'}{a^2 \mathcal{S}(\chi)^2}, \\ \varphi &= \varphi'_{\text{Sch\"uS}} + \arcsin \frac{T'_{\text{PS}}}{T(\chi)} - \gamma'_{\text{FLRW}}, \end{aligned} \quad (54)$$

with E' being a second constant of motion given by $E' := a'_{\text{Sch\"uS}} \dot{t}'_{\text{Sch\"uS}}$, involved, with J' (37), in the definition of the perilens χ'_{PS} such that \mathcal{S}'_{PS} , \mathcal{C}'_{PS} , and T'_{PS} are related to each other by $\mathcal{S}'_{\text{PS}} := \mathcal{S}(\chi'_{\text{PS}}) := J'/E'$, $\mathcal{C}'_{\text{PS}} := \mathcal{C}(\chi'_{\text{PS}}) := \sqrt{1 - kJ'^2/E'^2}$, $T'_{\text{PS}} := T(\chi'_{\text{PS}}) = \mathcal{S}'_{\text{PS}}/\mathcal{C}'_{\text{PS}}$, and γ'_{FLRW} is an angle defined by $\sin \gamma'_{\text{FLRW}} := T'_{\text{PS}}/T_{\text{Sch\"u}}$. It is noteworthy that one could easily check that γ'_{FLRW} represents the smaller physical angle between the unoriented direction of the upper photon and the direction toward the lens, i.e., $\gamma'_{\text{FLRW}} := \arctan(T_{\text{Sch\"u}} |d\varphi/d\chi|_{\text{Sch\"uS}})$.

Hence, the inclination angle of the source φ'_S corresponds to the geodesic distance between the lens to the source χ_{LS} (21), i.e.,

$$-\varphi'_S = -\varphi'_{\text{Sch\"uS}} - \arcsin \frac{T'_{\text{PS}}}{T_{\text{LS}}} + \gamma'_{\text{FLRW}}, \quad (55)$$

with $T_{\text{LS}} := T(\chi_{\text{LS}}) = \mathcal{S}_{\text{LS}}/\mathcal{C}_{\text{LS}}$, $\mathcal{S}_{\text{LS}} := \mathcal{S}(\chi_{\text{LS}})$, and $\mathcal{C}_{\text{LS}} := \mathcal{C}(\chi_{\text{LS}})$. Following the same reasoning as for the upper photon, one arrives at similar formulas for the lower photon, where only the constant J' differs from the first one by a minus sign. We restrict ourselves to giving the expression of the inclination angle φ_S ,

$$-\varphi_S = -\varphi_{\text{SchüS}} + \arcsin \frac{\mathcal{T}_{\text{PS}}}{\mathcal{T}_{\text{LS}}} - \gamma_{\text{FLRW}}, \quad (56)$$

which must be equal to φ'_S , since both photons are emitted by the same source, where $\mathcal{T}_{\text{PS}} := \mathcal{T}(\chi_{\text{PS}}) = \mathcal{S}_{\text{PS}}/\mathcal{C}_{\text{PS}}$, $\mathcal{S}_{\text{PS}} := \mathcal{S}(\chi_{\text{PS}}) := J/E$, $\mathcal{C}_{\text{PS}} := \mathcal{C}(\chi_{\text{PS}}) := \sqrt{1 - kJ^2/E^2}$, $E := a_{\text{SchüS}} \dot{t}_{\text{SchüS}}$, and $\sin \gamma_{\text{FLRW}} := \mathcal{T}_{\text{PS}}/\mathcal{T}_{\text{SchüS}}$.

However, these angles φ'_S and φ_S differ for randomly selected parameters. As explained in Ref. [15], of all the parameters involved, fitting the value of the lens mass turns out to be the only way to fulfil the required equality between them. Once the desired mass value is well established, we move to calculate the time delay thereafter.

Let us determine the scale factor a'_S at the emission time t'_S of the upper photon. Applying the same method followed in the Sec. III A, one finds easily an equation similar to (26) relating χ to the time, by using \mathcal{S}'_{PS} instead of \mathcal{S}'_{PE} ,

$$\frac{dt}{a(t)} = -\frac{d\chi}{h'(\chi)}, \quad h'(\chi) = \sqrt{1 - \frac{\mathcal{S}_{\text{PS}}'^2}{\mathcal{S}(\chi)^2}}, \quad (57)$$

where the minus sign ensures that χ decreases over time between the source and the vacuole. Similarly, integrating the right-hand side of the previous equation between χ_{LS} and $\chi_{\text{SchüS}}$, one arrives at

$$\int_{a'_S}^{a_{\text{SchüS}}} \frac{da}{a^2 H(a)} = k^{-1/2} \left(\arcsin \frac{\mathcal{C}_{\text{SchüS}}}{\mathcal{C}'_{\text{PS}}} - \arcsin \frac{\mathcal{C}_{\text{LS}}}{\mathcal{C}'_{\text{PS}}} \right), \quad (58)$$

which, through the use of the Friedmann equation, can be numerically solved for obtaining a'_S . Then, if one is interested in t'_S , it suffices us to use the Friedmann equation, i.e.,

$$t'_S = \int_{a_0}^{a'_S} \frac{da}{aH(a)}. \quad (59)$$

Likewise, the scale factor a_S and its corresponding emission time t_S of the lower photon are calculated by similar formulas to (58) and (59), replacing $a'_{\text{SchüS}}$ by $a_{\text{SchüS}}$, and χ'_{PS} by χ_{PS} .

Again, it is possible to proceed differently, such as in the flat and closed cases [10,15], by directly calculating the time delay through an approximate analytical expression, instead of calculating a_S and t_S separately. The idea consists of subtracting the two sides of (58) from their analogs of the lower photon and evaluating the integrals with respect to time. One gets

$$\int_{t'_{\text{SchüS}}}^{t_{\text{SchüS}}} \frac{dt}{a(t)} - \int_{t'_S}^{t_S} \frac{dt}{a(t)} = \arcsin \frac{\mathcal{C}_{\text{SchüS}}}{\mathcal{C}'_{\text{PS}}} - \arcsin \frac{\mathcal{C}_{\text{LS}}}{\mathcal{C}'_{\text{PS}}} - \arcsin \frac{\mathcal{C}_{\text{SchüS}}}{\mathcal{C}_{\text{PS}}} + \arcsin \frac{\mathcal{C}_{\text{LS}}}{\mathcal{C}_{\text{PS}}}. \quad (60)$$

As before, because the scale factor $a(t)$ varies noticeably only over cosmological timescales, the left-hand side of the above equation can be approximated as

$$\text{lhs} \simeq \frac{\Delta t_{\text{SchüS}}}{a'_{\text{SchüS}}} - \frac{\Delta t_S}{a'_S}. \quad (61)$$

TABLE I. Galaxy cluster mass M , position angle $-\varphi_S$, and time delay for the observed image pairs, (A, B) , (A, C) , (D, A) , (B, C) , and (D, C) of the lensed quasar SDSS J1004 + 4112 in flat Einstein-Straus-de Sitter space-time ($k = 0$). Bold values correspond to upper and lower limits.

Images	$(\Omega_{\Lambda 0}, \alpha, \alpha')$	$M[10^{13} M_{\odot}]$	$-\varphi_S[\mu]$	$\Delta t[\text{days}]$
(A, B)	$(+, +, +)$	2.735	0.2196	94
	$(+, -, +)$	2.709	0.3837	163
	$(\pm 0, \pm 0, \pm 0)$	2.706	0.2211	93
	$(-, +, -)$	2.702	0.0561	23
	$(-, -, -)$	2.677	0.2225	93
(A, C)	$(+, +, +)$	3.137	2.7878	1277
	$(+, -, +)$	3.108	2.9519	1346
	$(\pm 0, \pm 0, \pm 0)$	3.106	2.8069	1269
	$(-, +, -)$	3.103	2.6588	1192
	$(-, -, -)$	3.074	2.8252	1260
(D, A)	$(+, +, +)$	1.764	5.9872	2066
	$(+, -, +)$	1.738	6.1514	2108
	$(\pm 0, \pm 0, \pm 0)$	1.740	6.0282	2049
	$(-, +, -)$	1.742	5.9012	1991
	$(-, -, -)$	1.717	6.0675	2032
(B, C)	$(+, +, +)$	3.177	2.5682	1184
	$(+, -, +)$	3.147	2.7324	1254
	$(\pm 0, \pm 0, \pm 0)$	3.145	2.5858	1176
	$(-, +, -)$	3.143	2.4363	1099
	$(-, -, -)$	3.113	2.6027	1168
(D, C)	$(+, +, +)$	2.049	8.7749	3276
	$(+, -, +)$	2.019	8.9391	3314
	$(\pm 0, \pm 0, \pm 0)$	2.023	8.8350	3250
	$(-, +, -)$	2.026	8.7263	3186
	$(-, -, -)$	1.997	8.8926	3224

TABLE II. Uncertainties in the galaxy cluster mass M , the position angle $-\varphi_S$ and the time delay of the observed images, (A, B) , (B, C) , (A, C) , (D, A) , and (D, C) of the lensed quasar SDSS J1004 + 4112 in flat Einstein-Straus-de Sitter space-time ($k = 0$), with $\Delta\alpha := \alpha - \alpha'$.

Images	$\Delta\alpha(\mu)$	$M[10^{13} M_{\odot}]$	$-\varphi_S[\mu]$	$\Delta t[\text{days}]$
(A, B)	0.11	2.706 ± 0.029	$0.2211^{+0.1626}_{-0.1650}$	93 ± 70
(B, C)	1.25	3.145 ± 0.032	$2.5858^{+0.1466}_{-0.1495}$	1176^{+78}_{-77}
(A, C)	1.36	3.106 ± 0.032	$2.8069^{+0.1450}_{-0.1481}$	1269 ± 77
(D, A)	2.92	$1.740^{+0.024}_{-0.023}$	$6.0282^{+0.1232}_{-0.1270}$	2049^{+59}_{-58}
(D, C)	4.28	2.023 ± 0.026	$8.8350^{+0.1041}_{-0.1087}$	3250 ± 64

TABLE III. Variation of the galaxy cluster mass M , the position angle $-\varphi_S$, and the time delay Δt versus the cosmological constant Λ within its error bar $\pm 2.90744 \times 10^{-54} \text{ m}^{-2}$ for the observed image pairs (A, B) , (B, C) , (A, C) , (D, A) , and (D, C) of the lensed quasar SDSS J1004 + 4112 in flat Einstein-Straus-de Sitter space-time ($k = 0$). The angles α and α' are fixed in their central values.

Images	$(\Omega_{\Lambda 0}, \alpha, \alpha')$	$\delta\Lambda[\%]$	$M[10^{13}M_{\odot}]$	$\delta M[\%]$	$-\varphi_S[\eta]$	$\delta\varphi_S[\%]$	$\Delta t[\text{days}]$	$\delta\Delta t[\%]$
(A, B)	$(-, \pm 0, \pm 0)(+, \pm 0, \pm 0)$	5.33897	2.702196	0.271264	0.22251	-1.32403	93.0302	0.44038
			2.709526		0.21957		93.4399	
(B, C)			3.140887	0.271134	2.60266	-1.32411	1173.49	0.44219
			3.149403		2.56820		1178.68	
(A, C)			3.101231	0.271150	2.82518	-1.32398	1265.88	0.44253
			3.109640		2.78777		1271.49	
(D, A)			1.737773	0.271580	6.06753	-1.32362	2044.69	0.45774
			1.742492		5.98721		2054.05	
(D, C)			2.019884	0.271501	8.89263	-1.32376	3242.31	0.47344
			2.025368		8.77491		3257.66	

TABLE IV. Variation of the galaxy cluster mass M , the position angle $-\varphi_S$, and the time delay Δt versus the present curvature density Ω_{k0} within the range $[-0.3, 0.3]$ for the observed image pair (A, B) of the lensed quasar SDSS J1004 + 4112 in curved Einstein-Straus-de Sitter space-time ($k = \pm 1$). The angles α_A and α_B as well as the present dark energy density $\Omega_{\Lambda 0}$ are fixed in their central values.

(A, B)	$k = +1$				$k = -1$		
	$ \Omega_{k0} $	$M[10^{13}M_{\odot}]$	$-\varphi_S[\eta]$	$\Delta t[\text{days}]$	$M[10^{13}M_{\odot}]$	$-\varphi_S[\eta]$	$\Delta t[\text{days}]$
	0.0001	2.705905	0.221071	93.2337	2.706151	0.221158	93.2802
	0.0002	2.705775	0.221069	93.2284	2.706268	0.221243	93.3220
	0.0003	2.705646	0.221068	93.2236	2.706385	0.221328	93.3632
	0.0004	2.705516	0.221066	93.2184	2.706501	0.221414	93.4049
	0.0005	2.705386	0.221065	93.2131	2.706618	0.221499	93.4462
	0.0006	2.705256	0.221064	93.2083	2.706735	0.221584	93.4879
	0.0007	2.705128	0.221062	93.2030	2.706851	0.221670	93.5291
	0.0008	2.704997	0.221061	93.1977	2.706968	0.221755	93.5709
	0.0009	2.704867	0.221059	93.1925	2.707085	0.221841	93.6121
	0.001	2.704738	0.221058	93.1877	2.707202	0.221926	93.6539
	0.002	2.703442	0.221043	93.1359	2.708369	0.222782	94.0701
	0.003	2.702147	0.221029	93.0847	2.709538	0.223639	94.4874
	0.004	2.700854	0.221014	93.0335	2.710707	0.224499	94.9054
	0.005	2.699562	0.221000	92.9829	2.711877	0.225360	95.3251
	0.006	2.698271	0.220985	92.9317	2.713048	0.226223	95.7459
	0.007	2.696981	0.220971	92.8811	2.714219	0.227088	96.1680
	0.008	2.695692	0.220956	92.8299	2.715392	0.227955	96.5912
	0.009	2.694405	0.220941	92.7786	2.716565	0.228824	97.0156
	0.01	2.693118	0.220927	92.7280	2.717739	0.229694	97.4412
	0.02	2.680320	0.220780	92.2230	2.729522	0.238505	101.763
	0.03	2.667640	0.220632	91.7232	2.741385	0.247511	106.209
	0.04	2.655076	0.220482	91.2288	2.753326	0.256720	110.785
	0.05	2.642627	0.220332	90.7396	2.765345	0.266137	115.495
	0.06	2.630291	0.22018	90.2563	2.777441	0.275773	120.344
	0.07	2.618069	0.220028	89.7778	2.789613	0.285633	125.339
	0.08	2.605957	0.219875	89.3045	2.801859	0.295727	130.486
	0.09	2.593956	0.219720	88.8360	2.814178	0.306064	135.790
	0.1	2.582064	0.219566	88.3727	2.826569	0.316654	141.258
	0.2	2.468865	0.217984	83.9951	2.953836	0.438974	206.765
	0.3	2.365248	0.216372	80.0388	3.083522	0.60307	300.287

TABLE V. Variation of the galaxy cluster mass M , the position angle $-\varphi_S$, and the time delay Δt versus the present curvature density Ω_{k0} within the range $[-0.3, 0.3]$ for the observed image pair (B, C) of the lensed quasar SDSS J1004 + 4112 in curved Einstein-Straus-de Sitter space-time ($k = \pm 1$). The angles α_B and α_C as well as the present dark energy density $\Omega_{\Lambda 0}$ are fixed in their central values.

(B, C)	$k = +1$			$k = -1$		
$ \Omega_{k0} $	$M[10^{13}M_{\odot}]$	$-\varphi_S[\mu]$	$\Delta t[\text{days}]$	$M[10^{13}M_{\odot}]$	$-\varphi_S[\mu]$	$\Delta t[\text{days}]$
0.0001	3.145197	2.58578	1176.06	3.145484	2.58589	1176.23
0.0002	3.145046	2.58576	1176.00	3.145620	2.58599	1176.33
0.0003	3.144895	2.58574	1175.93	3.145757	2.58608	1176.43
0.0004	3.144744	2.58572	1175.87	3.145894	2.58618	1176.53
0.0005	3.144594	2.58571	1175.81	3.146030	2.58628	1176.63
0.0006	3.144443	2.58569	1175.74	3.146167	2.58637	1176.73
0.0007	3.144292	2.58567	1175.68	3.146303	2.58647	1176.83
0.0008	3.144141	2.58566	1175.61	3.146440	2.58656	1176.93
0.0009	3.143990	2.58564	1175.55	3.146576	2.58666	1177.03
0.001	3.143840	2.58562	1175.48	3.146713	2.58676	1177.13
0.002	3.142334	2.58545	1174.83	3.148080	2.58773	1178.12
0.003	3.140829	2.58528	1174.19	3.149447	2.58869	1179.12
0.004	3.139326	2.58511	1173.54	3.150816	2.58967	1180.12
0.005	3.137824	2.58494	1172.89	3.152185	2.59064	1181.13
0.006	3.136324	2.58477	1172.25	3.153556	2.59161	1182.13
0.007	3.134825	2.58460	1171.61	3.154927	2.59259	1183.14
0.008	3.133327	2.58443	1170.96	3.156300	2.59356	1184.15
0.009	3.131830	2.58426	1170.32	3.157673	2.59454	1185.16
0.01	3.130335	2.58409	1169.68	3.159047	2.59552	1186.17
0.02	3.115461	2.58237	1163.30	3.172843	2.60542	1196.39
0.03	3.100723	2.58064	1156.98	3.186733	2.61548	1206.80
0.04	3.086121	2.57890	1150.74	3.200718	2.62571	1217.40
0.05	3.071652	2.57714	1144.56	3.214797	2.63613	1228.20
0.06	3.057315	2.57537	1138.45	3.228968	2.64672	1239.21
0.07	3.043109	2.57359	1132.41	3.243231	2.65751	1250.43
0.08	3.029033	2.57179	1126.43	3.257585	2.66850	1261.87
0.09	3.015085	2.56999	1120.52	3.272027	2.67969	1273.53
0.1	3.001262	2.56818	1114.66	3.286557	2.69109	1285.43
0.2	2.869695	2.54969	1059.38	3.436029	2.81872	1419.22
0.3	2.749263	2.53084	1009.41	3.589010	2.98000	1588.39

Concerning the right-hand side, one gets up to the second-to-leading order in \mathcal{S}'_{PS} and \mathcal{S}_{PS} ($\sim 10^{-6}$) or in $\varphi'_{\text{SchüS}} - \varphi_S$ and $|\varphi_{\text{SchüS}} - \varphi_S|$ ($\sim 10^{-4}$) on account of (55) and (56),

$$\text{lhs} \simeq \frac{1}{2} \frac{(\varphi_{\text{SchüS}} - \varphi_S)^2 - (\varphi'_{\text{SchüS}} - \varphi_S)^2}{\mathcal{T}_{\text{Schü}}^{-1} - \mathcal{T}_{\text{LS}}^{-1}}. \quad (62)$$

Equating the two sides, one finally arrives at the expression of the total time delay

$$\Delta t \simeq a'_S \left[\frac{\Delta t_{\text{SchüS}}}{a'_{\text{SchüS}}} - \frac{1}{2} \frac{(\varphi_{\text{SchüS}} - \varphi_S)^2 - (\varphi'_{\text{SchüS}} - \varphi_S)^2}{\mathcal{T}_{\text{Schü}}^{-1} - \mathcal{T}_{\text{LS}}^{-1}} \right], \quad (63)$$

which is positive for $\alpha > \alpha'$. Obviously, this expression reproduces the time delays already calculated in Refs. [10, 15] in the flat and closed ESdS models, as well as that of the hyperbolic ESdS model,

$$\Delta t \simeq a'_S \left[\frac{\Delta t_{\text{SchüS}}}{a'_{\text{SchüS}}} - \frac{1}{2} \frac{(\varphi_{\text{SchüS}} - \varphi_S)^2 - (\varphi'_{\text{SchüS}} - \varphi_S)^2}{\coth(\chi_{\text{Schü}}) - \coth(\chi_{\text{LS}})} \right]. \quad (64)$$

Overall, we realize that the upper photon after being the first emitted by the source arrives at the vacuole earlier than the lower one, but in turn, comes out from it later in such a way as to be eventually received on Earth simultaneously with the lower photon. As a matter of fact, this happens because the upper photon, which takes the nearest path from the lens ($r'_p < r_p$), as illustrated in Fig. 1, more intensely experiences the space-time curvature around the lens mass.

For symmetry reasons, one can expect that the polar angle and the time delay cancel, $\varphi_S = 0$, $\Delta t = 0$, when $\alpha = \alpha'$, in which case the Earth and the lens, as well as the source are fully aligned to each other.

TABLE VI. Variation of the galaxy cluster mass M , the position angle $-\varphi_S$, and the time delay Δt versus the present curvature density Ω_{k0} within the range $[-0.3, 0.3]$ for the observed image pair (A, C) of the lensed quasar SDSS J1004 + 4112 in curved Einstein-Straus-de Sitter space-time ($k = \pm 1$). The angles α_A and α_C as well as the present dark energy density $\Omega_{\Lambda 0}$ are fixed in their central values.

(A, C)	$k = +1$			$k = -1$		
$ \Omega_{k0} $	$M[10^{13}M_{\odot}]$	$-\varphi_S[\mu]$	$\Delta t[\text{days}]$	$M[10^{13}M_{\odot}]$	$-\varphi_S[\mu]$	$\Delta t[\text{days}]$
0.0001	3.105487	2.80685	1268.67	3.105771	2.80696	1268.84
0.0002	3.105339	2.80683	1268.60	3.105906	2.80706	1268.94
0.0003	3.105190	2.80681	1268.53	3.106041	2.80715	1269.05
0.0004	3.105040	2.80679	1268.46	3.106176	2.80725	1269.15
0.0005	3.104892	2.80677	1268.39	3.106311	2.80735	1269.25
0.0006	3.104743	2.80675	1268.32	3.106446	2.80744	1269.36
0.0007	3.104594	2.80674	1268.25	3.106580	2.80754	1269.46
0.0008	3.104445	2.80672	1268.18	3.106716	2.80764	1269.56
0.0009	3.104296	2.80670	1268.11	3.106851	2.80773	1269.67
0.001	3.104147	2.80668	1268.04	3.106985	2.80783	1269.77
0.002	3.102661	2.8065	1267.34	3.108336	2.8088	1270.81
0.003	3.101175	2.80631	1266.64	3.109687	2.80976	1271.85
0.004	3.099691	2.80613	1265.94	3.111040	2.81073	1272.89
0.005	3.098208	2.80594	1265.25	3.112393	2.81170	1273.93
0.006	3.096726	2.80576	1264.55	3.113747	2.81268	1274.98
0.007	3.095246	2.80557	1263.85	3.115102	2.81365	1276.02
0.008	3.093767	2.80539	1263.16	3.116458	2.81463	1277.07
0.009	3.092290	2.80520	1262.47	3.117815	2.8156	1278.12
0.01	3.090814	2.80502	1261.77	3.119173	2.81658	1279.17
0.02	3.076127	2.80315	1254.89	3.132804	2.82646	1289.80
0.03	3.061575	2.80127	1248.08	3.146530	2.8365	1300.61
0.04	3.047157	2.79938	1241.34	3.160349	2.84671	1311.62
0.05	3.032870	2.79747	1234.68	3.174261	2.85709	1322.83
0.06	3.018715	2.79555	1228.08	3.188265	2.86765	1334.24
0.07	3.004688	2.79361	1221.56	3.202360	2.87839	1345.87
0.08	2.990789	2.79167	1215.11	3.216545	2.88932	1357.73
0.09	2.977018	2.78971	1208.73	3.230817	2.90046	1369.81
0.1	2.963370	2.78774	1202.41	3.245176	2.91179	1382.12
0.2	2.833462	2.76767	1142.76	3.392920	3.03827	1520.14
0.3	2.714550	2.74721	1088.85	3.544203	3.19707	1693.42

IV. APPLICATION TO THE LENSED QUASAR SDSS J1004 + 4112

The system SDSS J1004 + 4112 discovered in the Sloan Digital Sky Survey has a background source at a redshift $z_S = 1.734$, identified as a quasar lensed into five images, A, B, C, D , and E , by an intervening galaxy cluster at a redshift $z_L = 0.68$ [33–37]. The galaxy cluster is assumed to have a spherical inner structure, despite the fact that the presence of five images obviously violates this assumption. We find it convenient to express the observed position angles of images with respect to the galaxy cluster as

$$\begin{aligned}
\alpha_A &= 8''.37 \pm 0''.04, & \alpha_B &= 8''.48 \pm 0''.04, \\
\alpha_C &= 9''.73 \pm 0''.04, & \alpha_D &= 5''.45 \pm 0''.04, \\
\alpha_E &= 0''.21 \pm 0''.04, & &
\end{aligned} \tag{65}$$

where we have taken the same position angle error used in Refs. [38,39].

Throughout the application, we adopt, for the Hubble constant and the present dark energy density, a Λ CDM model's best-fit values provided by Planck collaboration [6]— $H_0 = (67.36 \pm 0.54) \text{ km s}^{-1} \text{ Mpc}^{-1}$ and $\Omega_{\Lambda 0} = 0.6847 \pm 0.0073$ —from which we deduce the cosmological constant value, $\Lambda = (1.08914 \pm 0.02907) \times 10^{-52} \text{ m}^{-2}$. Accordingly, the present matter and the present curvature densities are related by $\Omega_{\rho 0} = 0.3153 - \Omega_{k0}$.

A. Flat universe ($k = 0$)

We start by addressing the case without spatial curvature in order, *inter alia*, to appreciate discrepancies when the nonflat spaces will be considered afterward. The calculation of the source position angle $-\varphi_S$ using (55) or (56), and the time delay Δt using (63), for the image pairs (A, B) ,

TABLE VII. Variation of the galaxy cluster mass M , the position angle $-\varphi_S$, and the time delay Δt versus the present curvature density Ω_{k0} within the range $[-0.3, 0.3]$ for the observed image pair (D, A) of the lensed quasar SDSS J1004 + 4112 in curved Einstein-Straus-de Sitter space-time ($k = \pm 1$). The angles α_D and α_A as well as the present dark energy density $\Omega_{\Lambda 0}$ are fixed in their central values.

(D, A)	$k = +1$			$k = -1$		
$ \Omega_{k0} $	$M[10^{13}M_{\odot}]$	$-\varphi_S[\mu]$	$\Delta t[\text{days}]$	$M[10^{13}M_{\odot}]$	$-\varphi_S[\mu]$	$\Delta t[\text{days}]$
0.0001	1.740161	6.02817	2049.34	1.740321	6.02829	2049.58
0.0002	1.740078	6.02813	2049.22	1.740398	6.02837	2049.70
0.0003	1.739994	6.02809	2049.11	1.740475	6.02846	2049.83
0.0004	1.739911	6.02805	2048.99	1.740552	6.02854	2049.95
0.0005	1.739827	6.02801	2048.88	1.740628	6.02862	2050.08
0.0006	1.739744	6.02797	2048.76	1.740705	6.02870	2050.21
0.0007	1.739660	6.02793	2048.65	1.740782	6.02879	2050.33
0.0008	1.739577	6.02789	2048.54	1.740859	6.02887	2050.46
0.0009	1.739493	6.02785	2048.42	1.740936	6.02895	2050.58
0.001	1.739410	6.02781	2048.31	1.741012	6.02904	2050.71
0.002	1.738577	6.02741	2047.16	1.741781	6.02987	2051.97
0.003	1.737744	6.02702	2046.02	1.742550	6.03070	2053.23
0.004	1.736912	6.02662	2044.88	1.743320	6.03153	2054.49
0.005	1.736081	6.02622	2043.74	1.744090	6.03236	2055.76
0.006	1.735250	6.02583	2042.61	1.744861	6.03319	2057.02
0.007	1.734421	6.02543	2041.47	1.745632	6.03402	2058.29
0.008	1.733591	6.02503	2040.33	1.746404	6.03486	2059.56
0.009	1.732763	6.02463	2039.20	1.747177	6.03569	2060.83
0.01	1.731936	6.02423	2038.07	1.747950	6.03653	2062.11
0.02	1.723704	6.02022	2026.81	1.755712	6.04490	2074.93
0.03	1.715547	6.01617	2015.68	1.763531	6.05334	2087.92
0.04	1.707465	6.01209	2004.67	1.771406	6.06183	2101.09
0.05	1.699457	6.00799	1993.78	1.779338	6.07038	2114.43
0.06	1.691523	6.00385	1983.01	1.787325	6.07899	2127.96
0.07	1.683661	5.99969	1972.36	1.795368	6.08765	2141.67
0.08	1.675870	5.99550	1961.82	1.803466	6.09638	2155.57
0.09	1.668151	5.99129	1951.40	1.811618	6.10517	2169.67
0.1	1.660502	5.98706	1941.09	1.819824	6.11403	2183.96
0.2	1.587690	5.94388	1843.74	1.904550	6.20611	2338.84
0.3	1.521045	5.89987	1755.85	1.992164	6.30499	2519.23

(A, C) , (D, A) , (B, C) , and (D, C) , are carried out by fitting the galaxy cluster mass in function of maximum +, central ± 0 , and minimum $-$ values of $\Omega_{\Lambda 0}$, α , and α' . For convenience, the present scale factor a_0 is normalized to unity.² The results are displayed in Table I, where only some specific combinations of $(\Omega_{\Lambda 0}, \alpha, \alpha')$ within their error bars have been shown, corresponding to the upper, central, and lower limit values of M , $-\varphi_S$, and Δt , which are sufficient for estimating their uncertainties summarized in Table II.

At first sight, the Table II indicates that a small image angular difference $\Delta\alpha$ leads to a small polar angle $-\varphi_S$ as well as a small time delay and vice versa. This offers remarkably two important consequences. First, it concurs with our theoretical model which states that $-\varphi_S$ and Δt vanish for $\alpha = \alpha'$. Second, the reported time delays obey

²In the flat Universe, the present scale factor a_0 can be set arbitrarily without loss of generality.

the temporal ordering sequence $C-B-A-D$, where the longest and shortest time delays correspond to the longest and shortest angular differences $\Delta\alpha$ —the more widely separated C and D images and the more closely separated A and B images—respectively. This is all to say that a larger $\Delta\alpha$ leads to a larger $-\varphi_S$ as well as a longer Δt . The angular difference has then the same implications on the time delay hierarchy as it would be the case for the commonly used image angular separation. In particular, the broad range of time delays provides lower and upper bound estimates on the galaxy cluster mass, $1.717 \times 10^{13}M_{\odot} \leq M \leq 3.177 \times 10^{13}M_{\odot}$, or $M = (2.447 \pm 0.73) \times 10^{13}M_{\odot}$, which matches perfectly with the enclosed mass within a radius of 60 kpc, measured by Williams *et al.* ($\sim 2.5 \times 10^{13}M_{\odot}$) with Chandra x-ray observations, but roughly twice as small as their measurements within 100 kpc ($\sim 5 \times 10^{13}M_{\odot}$) [35,39–41]. Additionally, the time delay between A and B images is affected by a margin of uncertainty that is large

TABLE VIII. Variation of the galaxy cluster mass M , the position angle $-\varphi_S$, and the time delay Δt versus the present curvature density Ω_{k0} within the range $[-0.3, 0.3]$ for the observed image pair (D, C) of the lensed quasar SDSS J1004 + 4112 in curved Einstein-Straus-de Sitter space-time ($k = \pm 1$). The angles α_D and α_C as well as the present dark energy density $\Omega_{\Lambda 0}$ are fixed in their central values.

(D, C)	$k = +1$			$k = -1$		
$ \Omega_{k0} $	$M[10^{13}M_{\odot}]$	$-\varphi_S[\mu]$	$\Delta t[\text{days}]$	$M[10^{13}M_{\odot}]$	$-\varphi_S[\mu]$	$\Delta t[\text{days}]$
0.0001	2.022659	8.83494	3249.92	2.022846	8.8351	3250.3
0.0002	2.022562	8.83488	3249.74	2.022936	8.83519	3250.49
0.0003	2.022465	8.83483	3249.56	2.023026	8.83529	3250.69
0.0004	2.022368	8.83477	3249.37	2.023116	8.83539	3250.88
0.0005	2.022271	8.83471	3249.19	2.023206	8.83549	3251.07
0.0006	2.022174	8.83465	3249.00	2.023296	8.83558	3251.27
0.0007	2.022077	8.83459	3248.82	2.023386	8.83568	3251.46
0.0008	2.021981	8.83454	3248.64	2.023476	8.83578	3251.65
0.0009	2.021884	8.83448	3248.45	2.023566	8.83588	3251.85
0.001	2.021787	8.83442	3248.27	2.023656	8.83597	3252.04
0.002	2.020818	8.83384	3246.44	2.024556	8.83695	3253.97
0.003	2.019850	8.83326	3244.60	2.025457	8.83792	3255.91
0.004	2.018883	8.83268	3242.78	2.026359	8.83890	3257.85
0.005	2.017917	8.8321	3240.95	2.027261	8.83987	3259.79
0.006	2.016952	8.83151	3239.12	2.028164	8.84085	3261.74
0.007	2.015987	8.83093	3237.30	2.029068	8.84183	3263.68
0.008	2.015024	8.83035	3235.48	2.029972	8.8428	3265.63
0.009	2.014061	8.82976	3233.66	2.030877	8.84378	3267.58
0.01	2.013100	8.82918	3231.84	2.031783	8.84476	3269.54
0.02	2.003532	8.82330	3213.78	2.040877	8.85454	3289.21
0.03	1.994052	8.81737	3195.92	2.050039	8.86435	3309.14
0.04	1.984659	8.81140	3178.26	2.059270	8.87419	3329.31
0.05	1.975351	8.80538	3160.8	2.068568	8.88405	3349.75
0.06	1.966129	8.79932	3143.52	2.077934	8.89394	3370.44
0.07	1.956992	8.79322	3126.44	2.087367	8.90385	3391.41
0.08	1.947937	8.78709	3109.55	2.096867	8.91378	3412.64
0.09	1.938965	8.78092	3092.84	2.106432	8.92373	3434.16
0.1	1.930074	8.77472	3076.30	2.116063	8.93369	3455.96
0.2	1.845448	8.71147	2920.35	2.215671	9.03380	3690.85
0.3	1.767987	8.64699	2779.69	2.319147	9.13166	3960.63

enough to allow a plausible comparison with the results of Kawano and Oguri [37], $\Delta t_{AB} \lesssim 28$ days, and Fohlmeister *et al.* [36] $\Delta t_{AB} = (40.6 \pm 1.8)$ days. Our predicted time delays between B and C , and between D and C are further consistent with what Kawano and Oguri have obtained, $\Delta t_{BC} \lesssim 1400$ days, and $\Delta t_{DC} \lesssim 3700$ days. Fohlmeister *et al.* have used a mass model to predict a time delay of approximately 2000 days between D and A , in agreement with our result. The same authors have measured relative to the image pairs (B, C) and (A, C) , the following time delays: $\Delta t_{BC} = (782 \pm 7)$ days, $\Delta t_{AC} = (821.6 \pm 2.1)$ days, which are nonetheless quite shorter than our predictions. Likewise for Liu *et al.* who have lately reported in Ref. [42] time delays that differ from ours, but coincide with those of Muñoz *et al.* [43] and recent measurements by Perera *et al.* [41]: $\Delta t_{BC} = (781.92 \pm 2.20)$ days, $\Delta t_{AC} = (825.99 \pm 2.10)$ days, and $\Delta t_{DC} = (2456.99 \pm 5.55)$ days.

Failing to answer the question of what and how much is the effect of a positive Λ on the bending of light, we have made Table III, based upon the variation of the cosmological constant Λ within its error bar, from the lower value to the upper one, with keeping α and α' fixed in their central values. Quantitatively, all parameters are related monotonously to each other, but an increase of Λ by 5.34% leads to a relatively slight decrease of $-\varphi_S$ by 1.32% associated though with a very slightly increasing mass by 0.27%. The same values hold for all the image pairs. Even though the method is somewhat less robust than desired, the effect appears to be very small on cosmological scales. Note also that the time delay gets a relatively very slight increase as well: 0.44% for the image pairs (A, B) , (BC) , and (A, C) and 0.46% for (D, A) , and 0.47% for (D, C) , which are almost the same. While this statement has only been made in the framework of flat ESdS model, Hu *et al.* [29] have

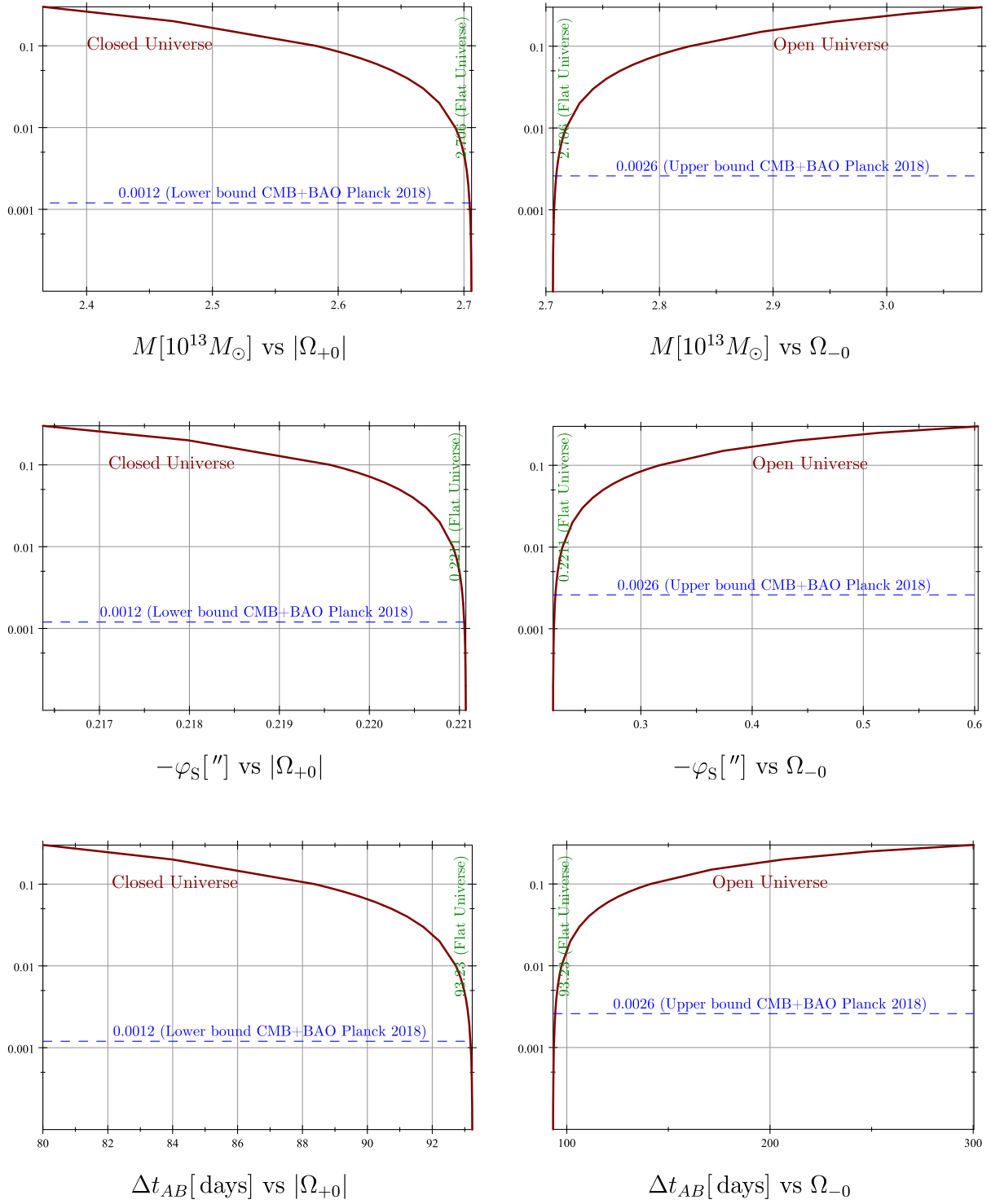


FIG. 2. Evolution of the galaxy cluster mass M , the position angle $-\varphi_S$, and the time delay Δt versus the present curvature density Ω_{k0} within the range $[-0.3, 0.3]$ for the observed image pair (A, B) of the lensed quasar SDSS J1004 + 4112 in curved Einstein-Straus-de Sitter space-time ($k = \pm 1$). The angles α_A and α_B as well as the present dark energy density $\Omega_{\Lambda 0}$ are fixed in their central values.

proceeded otherwise and more rigorously using a curved ESdS model in a simple case where the source is not inclined but aligned with both the lens and the observer. They isolate all affects that can be produced by other

parameters on the bending of light when varying Λ . Especially, they fix the angular diameter distance as well as the mass M and the radius of the vacuole by compensating the changes in $\Omega_{\Lambda 0}$ by Ω_{k0} . The calculations were

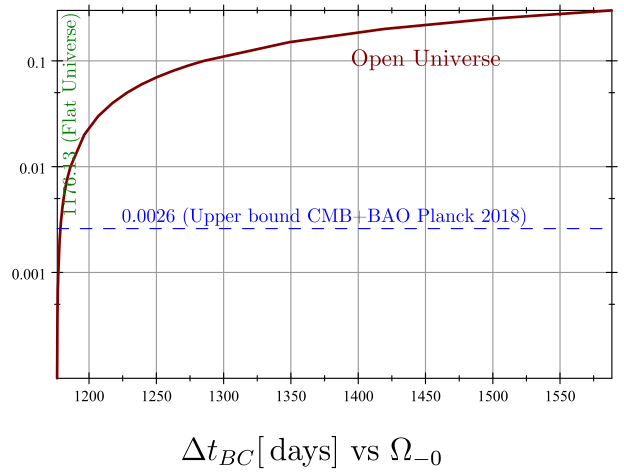
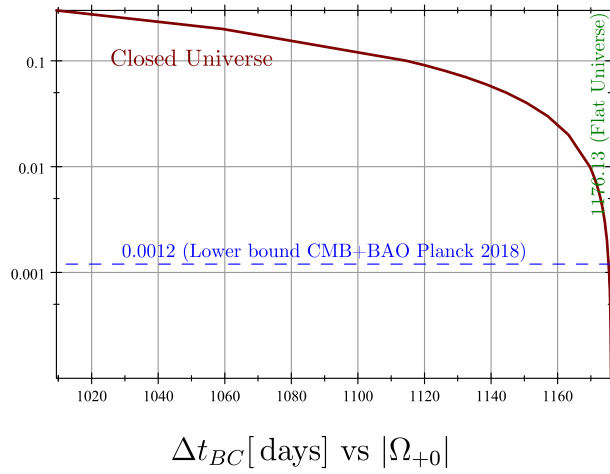
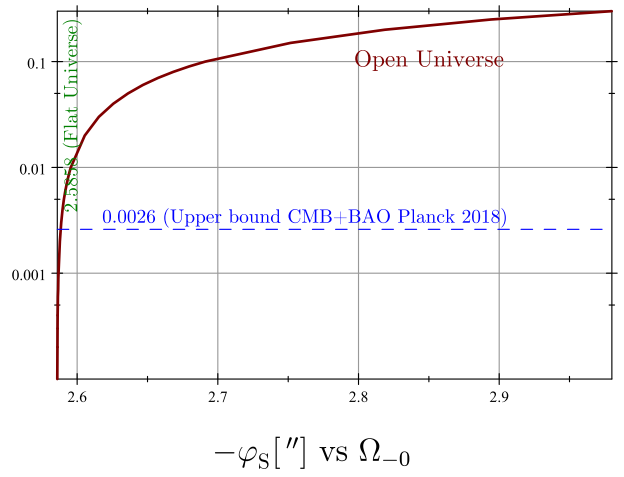
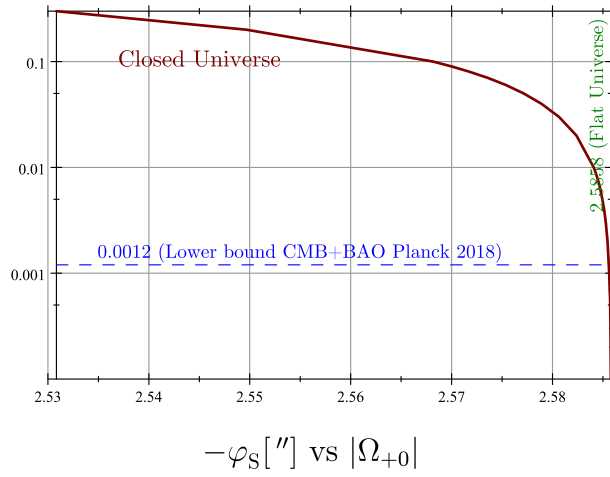
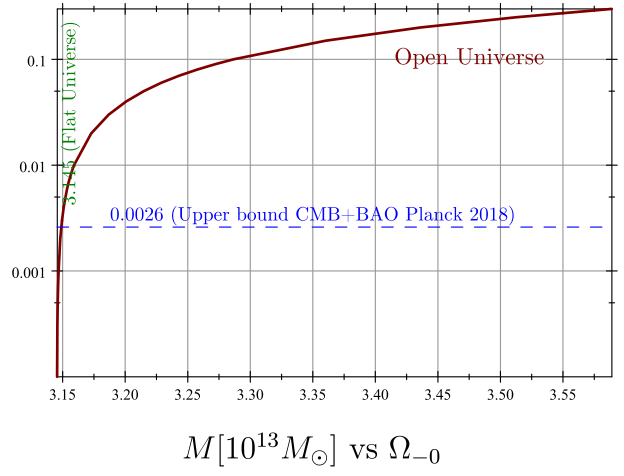
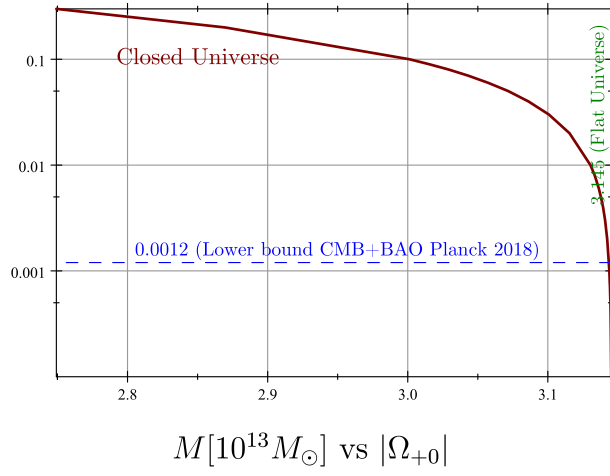


FIG. 3. Evolution of the galaxy cluster mass M , the position angle $-\varphi_S$, and the time delay Δt versus the present curvature density Ω_{k0} within the range $[-0.3, 0.3]$ for the observed image pair (B, C) of the lensed quasar SDSS J1004 + 4112 in curved Einstein-Strauss-de Sitter space-time ($k = \pm 1$). The angles α_B and α_C as well as the present dark energy density $\Omega_{\Lambda 0}$ are fixed in their central values.

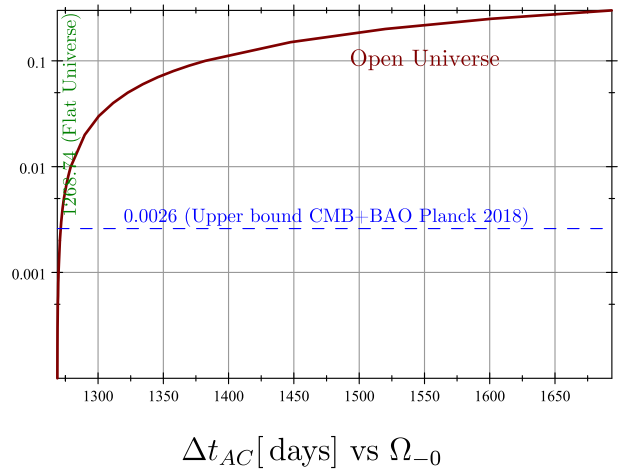
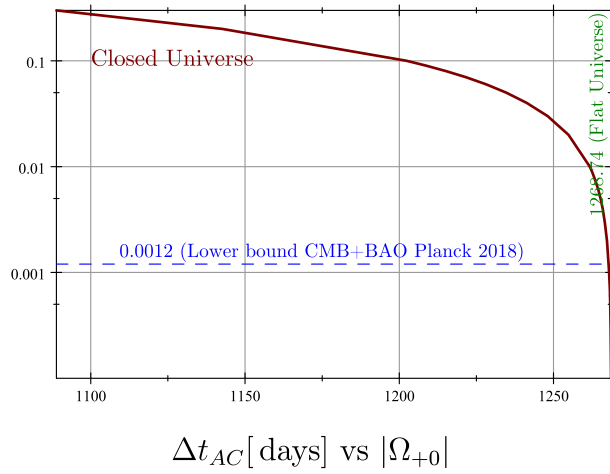
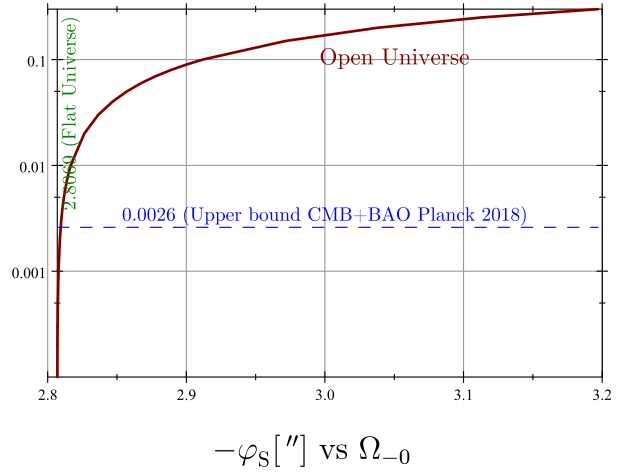
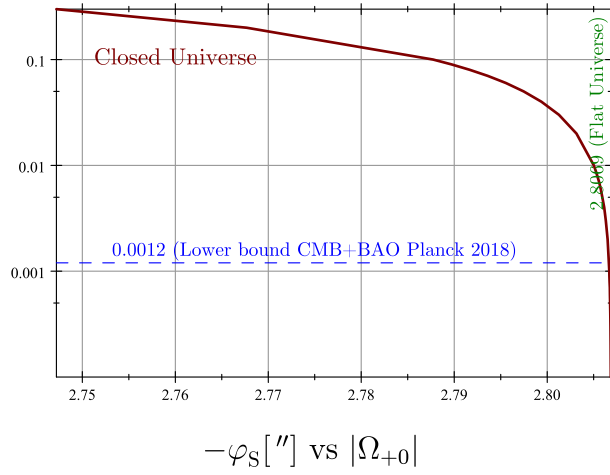
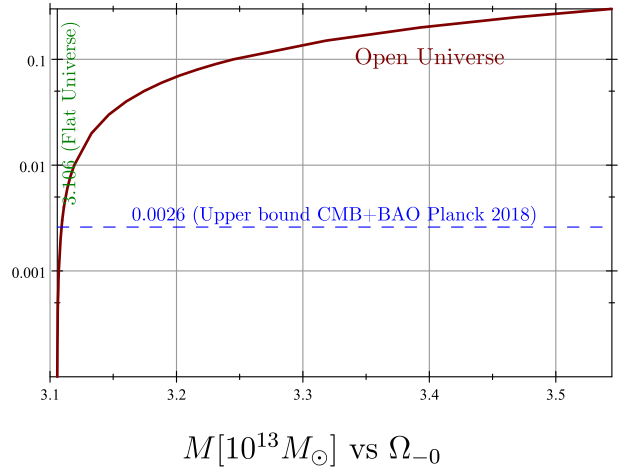
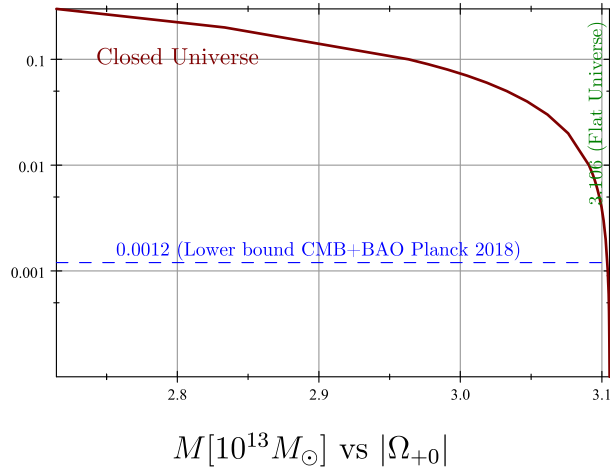


FIG. 4. Evolution of the galaxy cluster mass M , the position angle $-\varphi_S$, and the time delay Δt versus the present curvature density Ω_{k0} within the range $[-0.3, 0.3]$ for the observed image pair (A, C) of the lensed quasar SDSS J1004 + 4112 in curved Einstein-Strauss-de Sitter space-time ($k = \pm 1$). The angles α_A and α_C as well as the present dark energy density $\Omega_{\Lambda 0}$ are fixed in their central values.

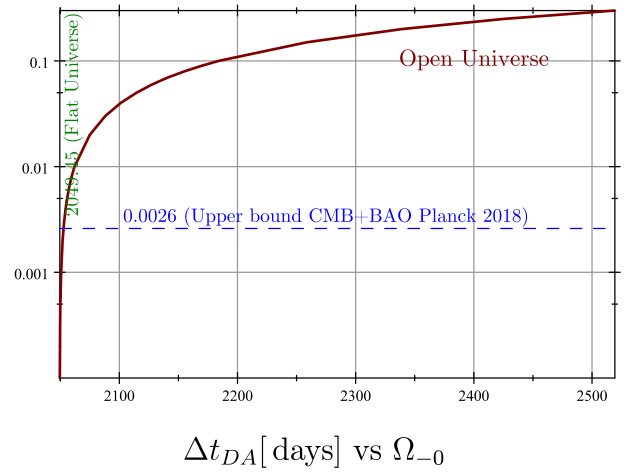
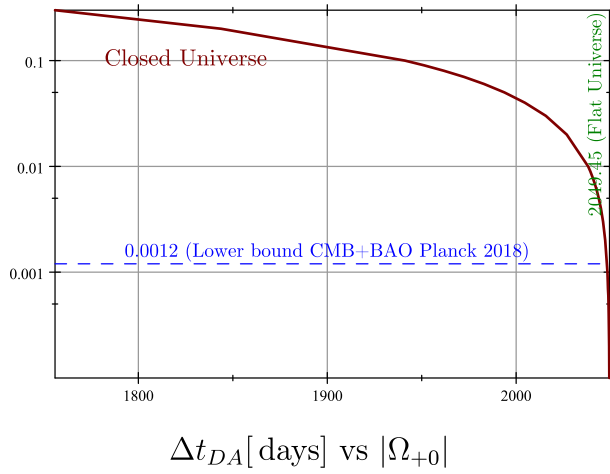
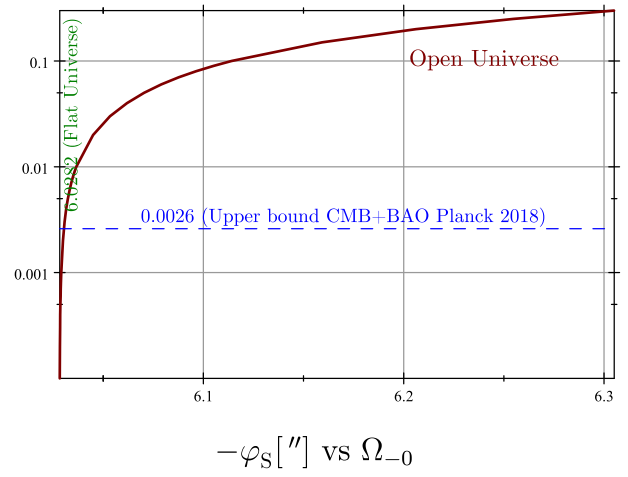
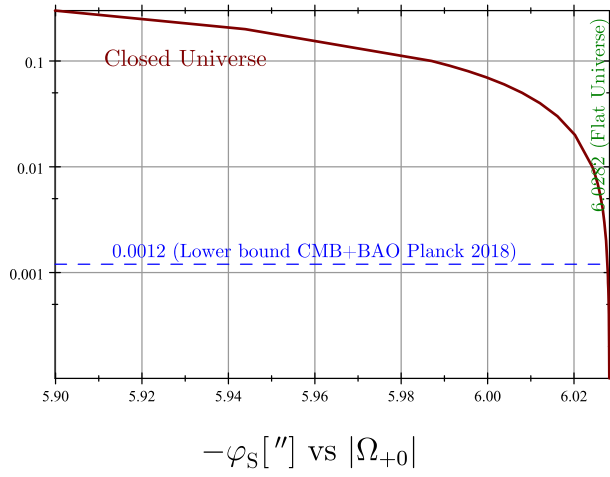
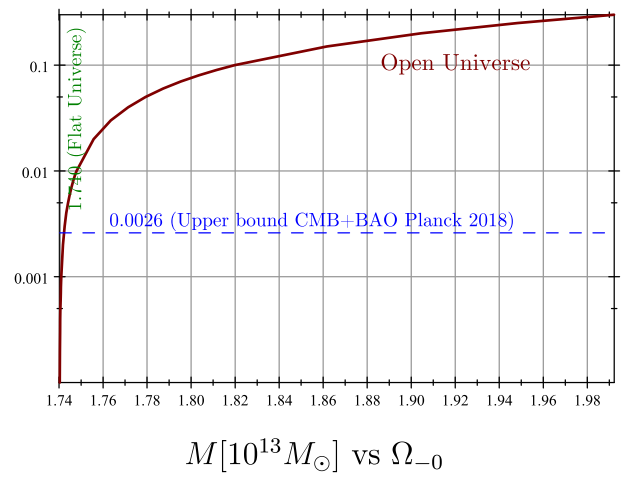
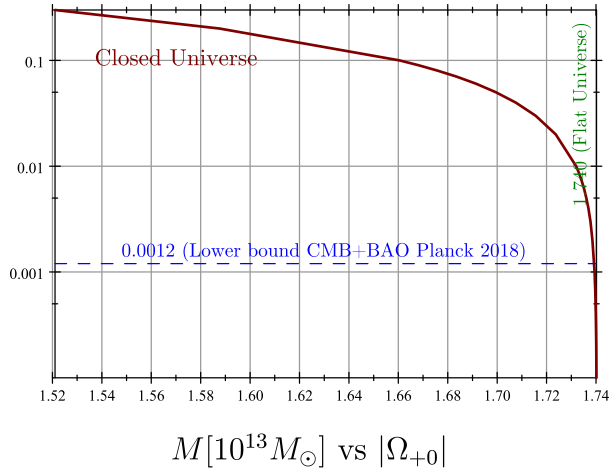
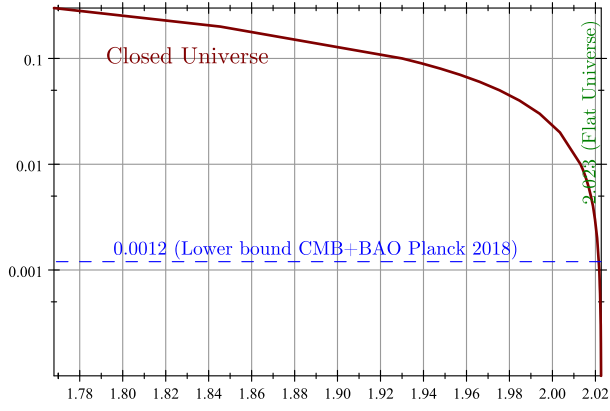
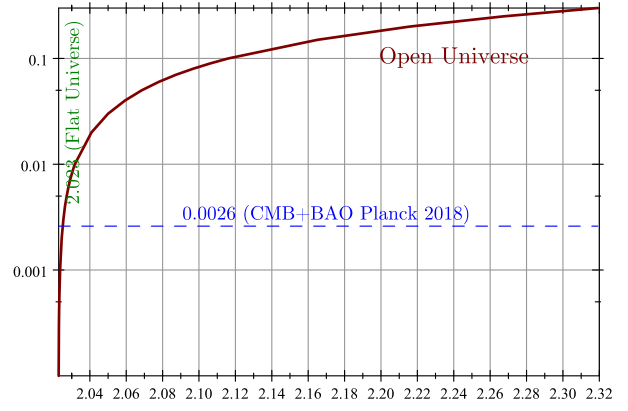


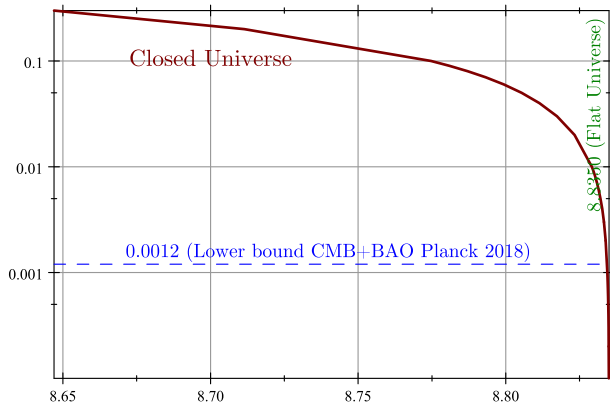
FIG. 5. Evolution of the galaxy cluster mass M , the position angle $-\varphi_S$, and the time delay Δt versus the present curvature density Ω_{k0} within the range $[-0.3, 0.3]$ for the observed image pair (D, A) of the lensed quasar SDSS J1004 + 4112 in curved Einstein-Straus-de Sitter space-time ($k = \pm 1$). The angles α_D and α_A as well as the present dark energy density $\Omega_{\Lambda 0}$ are fixed in their central values.



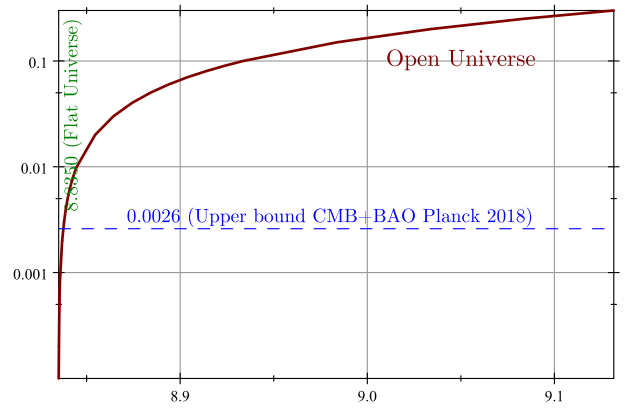
$M[10^{13} M_{\odot}]$ vs $|\Omega_{+0}|$



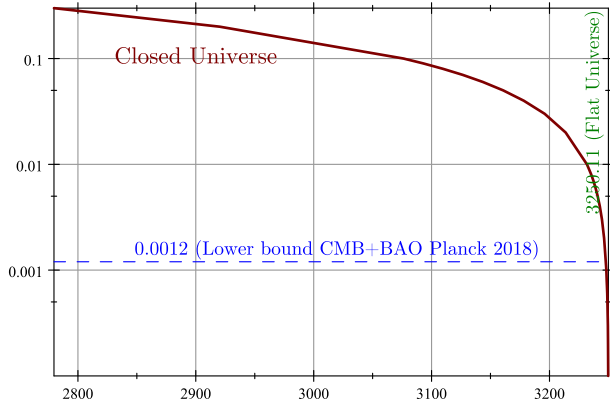
$M[10^{13} M_{\odot}]$ vs Ω_{-0}



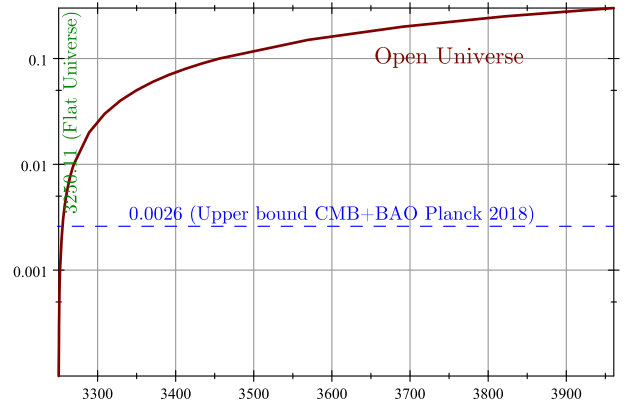
$-\varphi_S[']$ vs $|\Omega_{+0}|$



$-\varphi_S[']$ vs Ω_{-0}



$\Delta t_{DC}[\text{days}]$ vs $|\Omega_{+0}|$



$\Delta t_{DC}[\text{days}]$ vs Ω_{-0}

FIG. 6. Evolution of the galaxy cluster mass M , the position angle $-\varphi_S$, and the time delay Δt versus the present curvature density Ω_{k0} within the range $[-0.3, 0.3]$ for the observed image pair (D, C) of the lensed quasar SDSS J1004 + 4112 in curved Einstein-Strauss-de Sitter space-time ($k = \pm 1$). The angles α_D and α_C as well as the present dark energy density $\Omega_{\Lambda 0}$ are fixed in their central values.

performed for different masses and showed that the Λ effect on light bending is very tiny and can be neglected.

B. Positively curved universe ($k = +1$)

Now, we are going to study the effect of a positive spatial curvature on light deflection and time delay in the framework of a closed ESdS model. A better way to do this is to let the present curvature density Ω_{+0} free to vary discretely upon a set of $(\Omega_{\Lambda 0}, \alpha, \alpha')$ fixed in their central values. Thereupon, we fit the galaxy cluster mass for various values of Ω_{+0} , within the range $[-0.3, -0.0001]$,³ to calculate the polar angle $-\varphi_S$ and the time delay Δt of the four image pairs. The results are quoted in the Tables IV, V, VI, VII, and VIII. It would also be best to make use of plots, by interpolating the data points $(M, |\Omega_{+0}|)$, $(-\varphi_S, |\Omega_{+0}|)$, and $(\Delta t, |\Omega_{+0}|)$ separately. We note that inserting the logarithm function onto the y axis allows better visualization of the real effect in the vicinity of smaller $|\Omega_{+0}|$.

According to the Tables IV, V, VI, VII, and VIII, as well as the Figs. 2, 3, 4, 5, and 6, the galaxy cluster mass M , the polar angle $-\varphi_S$ as well as the time delay Δt follow the same behavior against the present curvature density $|\Omega_{+0}|$. Specifically, they decrease significantly upon increasing $|\Omega_{+0}|$ within its larger values. This is what the downward sloping part of graphs demonstrates. However, for smaller $|\Omega_{+0}|$, the parameters increase very slightly until they become steady. These limiting values through smaller $|\Omega_{+0}|$ are none other than those of the flat ESdS model in the Table I. These features remain the same regardless of which values are chosen for $\Omega_{\Lambda 0}$, α , and α' within their error bars. An added feature that is easy to check would be that the parameters M , $-\varphi_S$, and Δt are correlated almost linearly to each other through all the range of $|\Omega_{+0}|$. In view of this finding, we conclude that a small curvature density does not significantly impact the light deflection and the time delay.

C. Negatively curved universe ($k = -1$)

Analogously, we allow several values of Ω_{-0} within the range $[0.0001, 0.3]$ to show its impact on M , $-\varphi_S$ and Δt in the hyperbolic ESdS space-time. The results are reported in Tables IV, V, VI, VII, and VIII, and graphically presented in Figs. 2, 3, 4, 5, and 6. Conversely to the closed ESdS model, it is easy to see that the three parameters grow significantly upon increasing Ω_{-0} beyond its smaller values (the upward sloping part of graphs), whereas they decrease very slightly within smaller Ω_{-0} , until they become steady once reaching the parameter values of the flat ESdS model in the Table I. In this context one should note that this reverse effect is quite expected since the spatial curvature has changed its sign. Again, one can easily check that the

relationship between the parameters are approximately described by a linear function through all the range of Ω_{-0} . Finally, we have come to the same conclusion as for the closed Universe: including a small spatial curvature in the ESdS metric does not appreciably affect the light deflection and time delay.

V. CONCLUSION

In this work, we have generalized the computation of light deflection and time delay in the Einstein-Straus-de Sitter space-time, by modeling the gravitational lens as a static Schwarzschild-de Sitter vacuole embedded in an external FLRW Universe, with the purpose of covering together all three types of spatial curvature, $k = 0$ (flat Universe), $k = +1$ (closed Universe), and $k = -1$ (open Universe). This study results in generalized analytical expressions for the light deflection and the time delay.

After that, numerical applications to the lensed quasar SDSS J1004 + 4112 have been thoroughly performed for each case separately. Assuming first the flat Einstein-Straus-de Sitter background, predictions of five time delays between the four bright images of the aforementioned lensed quasar have been obtained and compared to some measurements in other research, (3250 ± 64) days for the well-known longest time delay between the images D and C , and (93 ± 70) days for the shortest one between the images A and B . For the other three time delays, we have gotten 2049_{-58}^{+59} days between the images D and A , (1269 ± 77) days between the images A and C , and 1176_{-77}^{+78} days between the images B and C . These time delays follow from the fit of the galaxy cluster mass for each image pair independently. The average mass that we have found is estimated to be $2.447 \times 10^{13} M_{\odot}$, with an accuracy of about 30%.

Additionally, we have shortly discussed the relationship between the light deflection and the cosmological constant and reached the following conclusion. Although the light deflection is attenuated in the presence of a positive cosmological constant, the results apparently seem to tell us that the effect is numerically less significant on cosmological scales, as has been recently asserted by Hu *et al.* [29]. The same conclusion holds for the time delay [11]. As for whether the instruments could observe this tiny effect, that is, in our view, another mission much more difficult.

After that, we have successively considered the Einstein-Straus-de Sitter model with positive and negative spatial curvature. A discrete variation of the present curvature density in the range $[-0.3, 0.3]$ is permitted to investigate its contribution to three parameters, the galaxy cluster mass, the light deflection, as well as the time delay. The results have been reported in tables, and graphically shown in figures, from which a number of conclusions have been drawn. Although the three parameters are linearly influenced by each other, assigning larger values to the present curvature density will impact them significantly. Clearly, the parameters are not subject to the same dependence on the modulus

³According to (5), the present curvature density is constrained by $\Omega_{k0} < 0.3153$, since the present matter density $\Omega_{\rho 0}$ must be positive definite.

of the present curvature density $|\Omega_{k0}|$ as it increases; they are decreasing in the closed Universe whereas they are increasing in the open Universe. This reversing effect is expected for cosmological models with different signs of curvature. However, the effect thereof is increasingly disappearing when the curvature density gets smaller and smaller $|\Omega_{k0}| \lesssim 0.001$, covering the parameters of the flat Universe. This characteristic holds true for both closed and open Einstein–Straus–de Sitter models. The precise value of the curvature density is currently still under active investigation, but if the observations truly trend in favor of small values thereof, one may feel confident saying that the expected small curvature of the current Universe is, as it were, not needed for the computation of light deflection and time delay in the Einstein–Straus–de Sitter model. On the other hand, in the cases where the present curvature density becomes important, this will profoundly influence the strong lensing phenomenon. These results indicate the robustness of our generalized approach, and, more importantly, they allow us to accurately constrain the spatial curvature on the basis of observational light deflection and time delay data.

To our knowledge, very little research tackles the question of Ω_{k0} effect on gravitational lensing. The author of Ref. [44] exploits weak-lensing data to constrain the curvature density on which the angular diameter distance between the lens and the source depends. A similar study is carried out in Ref. [45]. In Ref. [46], it was shown that the supernova light-curve parameters are unaffected by the curvature density. In Ref. [47], a closed Universe has been considered to analyze the evolution of the dark energy and

matter densities against Ω_{k0} , demonstrating that the only conceivable values correspond to small curvature densities. The dependence of the gravitational potential on the spatial curvature in the weak field limit has been proved in Ref. [48], using the same cosmological parameters as ours with realistic small curvature densities [6]. Finally, in Ref. [49], the authors have derived a particular local static FLRW metric from the osculating de Sitter metric, concluding that the spatial curvature effects on the local dynamics are minor but may not be negligible.

Recently in Ref. [41], Perera *et al.* have estimated a shorter time delay of roughly 8 yr between the image *C* and the faint fifth image *E* [50], very close to what Forés-Toribio *et al.* have obtained before [39], and a longer one of roughly 9 yr. We have overlooked the image *E* in this work owing to the fact that fitting the cluster mass is not possible or yields values that are far from acceptable. The image in question is located very close to the center of the galaxy cluster (~ 0.2 arcsec) (65), meaning that the associated photon inevitably encounters the mass distribution along the path. While it may depend on the nonspherical mass distribution, to which the photon is more sensitive, we think including an interior Schwarzschild–de Sitter solution [51] to the Einstein–Straus–de Sitter model would likely be a possible route to circumvent this problem. We are currently challenging ourselves to respond to this question in the hope it will be issued in the near future. Another avenue to test whether our findings are reliable would be to expand our analysis to cover other lensed quasar systems.

-
- [1] A. Einstein and E. G. Straus, The influence of the expansion of space on the gravitation fields surrounding the individual star, *Rev. Mod. Phys.* **17**, 120 (1945).
 - [2] A. Einstein and E. G. Straus, Corrections and additional remarks to our paper: The influence of the expansion of space on the gravitation fields surrounding the individual stars, *Rev. Mod. Phys.* **18**, 148 (1946).
 - [3] E. Schücking, Das Schwarzschildsche Linienelement und die expansion des Weltalls, *Z. Phys.* **137**, 595 (1954).
 - [4] R. Balbinot, R. Bergamini, and A. Comastri, Solution of the Einstein–Strauss problem with a Λ term, *Phys. Rev. D* **38**, 2415 (1988).
 - [5] M. Mars, F. C. Menay, and R. Vera, Review on exact and perturbative deformations of the Einstein–Straus model: Uniqueness and rigidity results, *Gen. Relativ. Gravit.* **45**, 2143 (2013).
 - [6] N. Aghanim *et al.* (Planck Collaboration), Planck 2018 results. VI. Cosmological parameters, *Astron. Astrophys.* **641**, A6 (2020).
 - [7] M. Ishak, Light deflection, lensing, and time delays from gravitational potentials and Fermat’s principle in the presence of a cosmological constant, *Phys. Rev. D* **78**, 103006 (2008).
 - [8] T. Schücker, Strong lensing in the Einstein–Straus solution, *Gen. Relativ. Gravit.* **41**, 1595 (2009).
 - [9] R. Kantowski, B. Chen, and X. Dai, Gravitational lensing corrections in flat Λ CDM cosmology, *Astrophys. J.* **718**, 913 (2010).
 - [10] K.-E. Boudjemaa, M. Guenouche, and S. R. Zouzou, Time delay in the Einstein–Straus solution, *Gen. Relativ. Gravit.* **43**, 1707 (2011).
 - [11] B. Chen, R. Kantowski, and X. Dai, Time delay in Swiss cheese gravitational lensing, *Phys. Rev. D* **82**, 043005 (2010).
 - [12] B. Chen, R. Kantowski, and X. Dai, Gravitational lens equation for embedded lenses; magnification and ellipticity, *Phys. Rev. D* **84**, 083004 (2011).
 - [13] R. Kantowski, B. Chen, and X. Dai, Image properties of embedded lenses, *Phys. Rev. D* **86**, 043009 (2012).

- [14] R. Kantowski, B. Chen, and X. Dai, Fermat's least-time principle and the embedded transparent lens, *Phys. Rev. D* **88**, 083001 (2013).
- [15] M. Guenouche and S. R. Zouou, Deflection of light and time delay in closed Einstein-Straus solution, *Phys. Rev. D* **98**, 123508 (2018).
- [16] W. Rindler and M. Ishak, Contribution of the cosmological constant to the relativistic bending of light revisited, *Phys. Rev. D* **76**, 043006 (2007).
- [17] M. Ishak, W. Rindler, J. Dossett, J. Moldenhauer, and C. Allison, A new independent limit on the cosmological constant/dark energy from the relativistic bending of light by galaxies and clusters of galaxies, *Mon. Not. R. Astron. Soc.* **388**, 1279 (2008).
- [18] M. Sereno, Influence of the cosmological constant on gravitational lensing in small systems, *Phys. Rev. D* **77**, 043004 (2008).
- [19] T. Schücker, Cosmological constant and lensing, *Gen. Relativ. Gravit.* **41**, 67 (2009).
- [20] I. B. Khriplovich and A. A. Pomeransky, Does the cosmological term influence gravitational lensing?, *Int. J. Mod. Phys. D* **17**, 2255 (2008).
- [21] M. Park, Rigorous approach to gravitational lensing, *Phys. Rev. D* **78**, 023014 (2008).
- [22] T. Schücker, Strong lensing with positive cosmological constant, [arXiv:0805.1630](https://arxiv.org/abs/0805.1630).
- [23] M. Sereno, Role of Λ in the cosmological lens equation, *Phys. Rev. Lett.* **102**, 021301 (2009).
- [24] F. Simpson, J. A. Peacock, and A. F. Heavens, On lensing by a cosmological constant, *Mon. Not. R. Astron. Soc.* **402**, 2009 (2010).
- [25] H. Miraghaei and M. Nouri-Zonoz, Classical tests of general relativity in the Newtonian limit of Schwarzschild-de Sitter spacetime, *Gen. Relativ. Gravit.* **42**, 2947 (2010).
- [26] T. Schücker, Lensing in the Einstein-Straus solution, [arXiv:1006.3234](https://arxiv.org/abs/1006.3234).
- [27] J. Sultana, Contribution of the cosmological constant to the bending of light in Kerr-de Sitter spacetime, *Phys. Rev. D* **88**, 042003 (2013).
- [28] M. Heydari-Fard, M. Heydari-Fard, and H. R. Sepang, Bending of light in novel 4D Gauss-Bonnet-de Sitter black holes by the Rindler-Ishak method, *Europhys. Lett.* **133**, 50006 (2021).
- [29] L. Hu, A. Heavens, and D. Bacon, Light bending by the cosmological constant, *J. Cosmol. Astropart. Phys.* **02** (2022) 009.
- [30] J. Sultana, Comment on "Gravitational lensing in Weyl gravity", *Phys. Rev. D* **108**, 108501 (2023).
- [31] J. Sultana, Gravitational light bending in Weyl gravity and Schwarzschild-de Sitter spacetime, *Symmetry* **16**, 101 (2024).
- [32] T. Schücker and N. Zaimen, Cosmological constant and time delay, *Astron. Astrophys.* **484**, 103 (2008).
- [33] N. Inada *et al.*, A gravitationally lensed quasar with quadruple images separated by 14.62 arcseconds, *Nature (London)* **426**, 810 (2003).
- [34] M. Oguri *et al.*, Observations and theoretical implications of the large separation lensed quasar SDSS J1004 + 4112, *Astrophys. J.* **605**, 78 (2004).
- [35] N. Ota *et al.*, Chandra observations of SDSS J1004 + 4112: Constraints on the lensing cluster and anomalous X-ray flux ratios of the quadruply imaged quasar, *Astrophys. J.* **647**, 215 (2006).
- [36] J. Fohlmeister, C. S. Kochanek, E. E. Falco, C. W. Morgan, and J. Wambsganss, The rewards of patience: An 822 day time delay in the gravitational lens SDSS J1004 + 4112, *Astrophys. J.* **676**, 761 (2008).
- [37] Y. Kawano and M. Oguri, Time delays for the giant quadruple lensed SDSS J1004 + 4112: Prospects for determining the density profile of the lensing cluster, *Publ. Astron. Soc. Jpn.* **58**, 271 (2006).
- [38] M. Oguri, The mass distribution of SDSS J1004 + 4112 revisited, *Publ. Astron. Soc. Jpn.* **62**, 1017 (2010).
- [39] R. Forés-Toribio, J. A. Muñoz, C. S. Kochanek, and E. Mediavilla, A mass model for the lensing cluster SDSSJ1004 + 4112: Constraints from the third time delay, *Astrophys. J.* **937**, 35 (2022).
- [40] L. L. R. Williams and P. Saha, Models of the giant quadruple quasar SDSSJ1004 + 4112, *Astron. J.* **128**, 2631 (2004).
- [41] D. Perera *et al.*, Free-form and hybrid lens models for SDSS J1004 + 4112: Substructure and central image time delay constraints, *Mon. Not. R. Astron. Soc.* **527**, 2639 (2024).
- [42] Y. Liu, M. Oguri, and S. Cao, Hubble constant from the cluster-lensed quasar system SDSS J1004 + 4112: Investigation of the lens model dependence, *Phys. Rev. D* **108**, 083532 (2023).
- [43] J. Muñoz, C. S. Kochanek, J. Fohlmeister, J. Wambsganss, E. Falco, and R. Forés-Toribio, The longest delay: A 14.5 yr campaign to determine the third time delay in the lensing cluster SDSS J1004 + 4112, *Astrophys. J.* **937**, 34 (2022).
- [44] G. Bernstein, Metric tests for curvature from weak lensing and baryon acoustic oscillations, *Astrophys. J.* **637**, 598 (2006).
- [45] K. Liao, Constraints on cosmic curvature with lensing time delays and gravitational waves, *Phys. Rev. D* **99**, 083514 (2019).
- [46] J.-J. We and X.-F. Wu, An improved method to measure the cosmic curvature, *Astrophys. J.* **838**, 160 (2017).
- [47] U. França, Dark energy, curvature, and cosmic coincidence, *Phys. Lett. B* **641**, 351 (2006).
- [48] M. Eingorn, A. E. Yükselci, and A. Zhuk, Effect of the spatial curvature of the Universe on the form of the gravitational potential, *Eur. Phys. J. C* **79**, 655 (2019).
- [49] M. Mizony and M. Lachièze-Rey, Cosmological effects in the local static frame, *Astron. Astrophys.* **434**, 45 (2005).
- [50] N. Inada *et al.*, Discovery of a fifth image of the large separation gravitationally lensed quasar SDSS J1004 + 4112, *Publ. Astron. Soc. Jpn.* **57**, L7 (2005).
- [51] T. Schücker, Lensing in an interior Kottler solution, *Gen. Relativ. Gravit.* **42**, 1991 (2010).